The Pennsylvania State University

The Graduate School

Department of Meteorology

MODELING STUDIES OF THE TRANSPORT AND TRANSFORMATION OF POLLUTANTS IN THE LOWER TROPOSPHERE

A Thesis in

Meteorology

by

Ariel F. Stein

Submitted in Partial Fulfillment
of the Requirements
for the Degree of

Doctor of Philosophy

December 2001

We approve the thesis of Ariel F. Stein.

Date of Signature

Dennis Lamb
Professor of Meteorology
Thesis Advisor
Chair of Committee

William H. Brune
Professor of Meteorology
Head of the Department of Meteorology

Gregory S. Jenkins
Assistant Professor of Meteorology

Brian A. Dempsey
Professor of Environmental Engineering

ABSTRACT

The utilization of mathematical models to represent the fates and transformations of atmospheric pollutants constitutes a fundamental practice that has contributed to the conceptual understanding of a variety of phenomena. These models provide the necesary framework for incorporating diverse atmospheric processes into a coherent system for studying their interactions. Consequently, we use several increasingly complex simulation tools to comprehend different aspects of pollution phenomena, such as the dispersion of non-reacting pollutants emitted from a smokestack, the forecast of tropospheric ozone formation over a regional scale, and the sensitivity of sulfate aerosol to changes in nitrogen oxides and hydrocarbon source strengths.

Starting with the simplest approach for simulating the dispersion of a chemically non-reactive contaminant, we explore the comparability of Gaussian-type model predictions to atmospheric measurements. This work investigates the differences between time-averaged observations and ensemble mean concentrations as predicted by Gaussian models in laboratory and atmospheric boundary layer (ABL) flows. For a given averaging time it is shown that this difference is smaller in laboratory flows than in the ABL under the same stability and statistical conditions. Furthermore, with data from the Willis-Deardorff convection tank experiments, it is shown that the values of the normalized differences between observations and model-predicted concentrations in the ABL exceed 50 % for an averaging time of the order of 1 hour. These findings give a

clear indication of the need for development of more accurate and sophisticated modeling tools to depict the atmospheric dispersion of non-reactive pollutants.

In view of the fact that Gaussian models show high discrepancies between modeled and observed concentrations and that this approach is unable to simulate the formation of secondary pollutants, it is necessary to increase the level of complexity to model phenomena such as photochemical smog. Thus, a three-dimensional model, the Hybrid Single-Particle Lagrangian Integrated Trajectories model with a generalized non-linear Chemistry Module (HY-SPLIT CheM), has been utilized to forecast summertime ozone concentrations over the northeastern United States. The ability of HY-SPLIT CheM to simulate ozone mixing ratios has been evaluated by comparing calculated summertime ozone mixing ratios against measured values for the month of July, 1999. Generally, a fair agreement is observed at most stations, especially taking into account the large number of assumptions used to construct the model. HY-SPLIT CheM is the first operational implementation of the particle-in-grid approach applied to air quality modeling. This model constitutes a feasible tool due to its simplicity and low cost of implementation.

The study of the formation of aerosol particles, specifically sulfate (SO_4^{2-}) aerosols, involves a complicated coupling among gas-phase chemical reactions (as in the formation of ozone), aqueous-phase photochemical, and meteorological processes within the simulation framework. The formation of SO_4^{2-} is chemically linked to primary emissions of sulfur dioxide (SO_2) via atmospheric oxidants and therefore also to the emissions of nitrogen oxides (NO_x) and volatile organic compounds (VOC). These

compounds represent the chemical precursors of ozone, which in turn constitutes the main source of SO_2 oxidants.

The response of SO_4^{2-} production to controls in NO_x and VOC emissions depends in part on the resulting changes in oxidant levels and the competition that naturally exists between the gas- and aqueous-phase pathways for SO_2 oxidation. We therefore propose the use of a combination of concentrations of nitric acid, particulate nitrate, hydrogen peroxide, and sulfate as a non-dimensional indicator of the effectiveness of VOC or NO_x controls in decreasing SO_4^{2-} abundance. The concentrations of these indicator species were calculated from a series of photochemical model simulations with varying rates of NO_x and VOC emissions using a state-of-the-art three-dimensional Eulerian model (MODELS-3) that covers the northeastern United States. It is shown that sulfate concentrations are likely to decrease as VOC emissions are reduced when the non-dimensional indicator is less than about 1.5. Under these same conditions a reduction in NO_x emissions would, however tend to *increase* the SO_4^{2-} levels. On the other hand, a higher value of the indicator identifies a regime in which reductions in NO_x emissions are more effective for reducing sulfate than VOC emissions are. In addition, a description of the sulfate-formation pathways, along with a theoretical analysis of the transition between NO_x- and VOC-sensitive regimes, provides a strong rationale for the use of the sulfate-sensitivity indicator.

TABLE OF CONTENTS

LIST OF FIGURES

LIST OF TABLES

ACKNOWLEDGMENTS

This thesis was supported in various parts by the US National Oceanic and Atmospheric Administration under NOAA contract Nos. 50-EANR-5-00033 and 50-EANR-1-00019. I would like to thank the members of my thesis committee Dr. William Brune, Dr. Gregory Jenkins and Dr. Brian Dempsey for helpful comments and discussions. The help of Roland Draxler and Rick Artz is greatly appreciated. I also acknowledge Dr. John Wyngaard for his academic and human support. I am very thankful to my adviser, Dr. Dennis Lamb, for letting me grow free and transmitting his passion for science.

To my family and friends,

Agradezco a mis amigos Luis, Mari, Flaco, Viri, Santi, Menchu, Ceci, y Pablo por su apoyo constante. A Josi que esta despertando hacia el camino del pensamiento cientifico. A Sole y Valentin quienes representan el futuro. Gracias a mi mamá quien con su afecto me sostuvo en todo momento. Agradezco a mi papá por ser mi fuente constante de inspiracion y orgullo. A Claudio, hermano del alma, muchas gracias por tu cariño y por demostrarme que vale la pena seguir adelante.

A mi compañera de vida, Any, le debo un agradecimiento especial ya que gran parte de esta tesis ha sido generada gracias a ella. Te agradezco amor por tu paciencia y dulzura, por estar a mi lado en cada momento y por sentirme a salvo cuando me abrazás.

Chapter 1

INTRODUCTION

The atmosphere constitutes an extremely complex system in which numerous physical and chemical processes take place at the same time. An understanding of individual atmospheric processes, typically achieved through laboratory experimentation or ambient-air measurements, is necessary, but it does not imply a global comprehension of the system. Mathematical models provide the necessary framework for incorporating the discrete atmospheric processes into a coherent system for studying their interactions. There is thus a close relationship among laboratory experiments, ambient-air measurements and atmospheric models. Laboratory studies generally focus on a particular process and provide parameters needed by the models, ambient-air monitoring identifies the state of the atmosphere and provides data for evaluation of atmospheric simulations, and atmospheric models integrate a conceptual understanding of atmospheric processes (Seinfeld and Pandis, 1998, p. 1193).

This thesis comprises three main studies that involve the use of ambient measurements and atmospheric modeling with increasing degrees of complexity. Departing from the simplest air pollution phenomenon to model, we study the atmospheric dispersion of a non-reacting pollutant released from a smokestack. This first

investigation deals particularly with Gaussian plume models and the comparability of their predictions to atmospheric measurements. Increasing the level of complexity, the second work explores the interactions between clear-air chemical and meteorological processes using a three-dimensional hybrid Lagrangian-Eulerian model to forecast summertime tropospheric ozone concentrations over the regional scale. Finally, the third study involves modeling of gas- and aqueous-phase chemical reactions and their interactions with synoptic meteorological processes. Consequently, aerosol sulfate formation is investigated using a state-of-the-art modeling tool and indicators of sulfate sensitivity to changes in the emissions of nitrogen oxides and hydrocarbons are developed.

Atmospheric dispersion models are fundamental tools in regulatory decision making and pollution control. In particular, Gaussian-plume models are widely used in a variety of environmental assessment applications, such as in the permitting process for facilities emitting air pollutants. Given the control costs associated with those practices, it is important to know the limitations and accuracy of these models. Venkatram (1988) identified the causes of air quality model uncertainty as errors in model inputs, errors in model formulation, and “inherent uncertainty” associated with the stochastic nature of turbulence. While the first and second contributions can in principle be reduced, it has been recognized that inherent uncertainty typically constitutes a major fraction of the total uncertainty (Fox 1984).

The standard Gaussian-plume modeling approach assumes that under steady-state meteorological conditions and constant emission rate, the dispersion of a non-reactive

effluent results in a mean downwind concentration field that has a Gaussian profile in the horizontal and in the vertical. The mean here is the ensemble mean, defined as the average over a large collection of events governed by a similar set of externally imposed conditions (Venkatram, 1984). Such a mean could be taken as a sufficiently long time average under statistically steady conditions. But the dispersion of pollutants in the turbulent atmospheric boundary layer is a stochastic phenomenon, and observations vary in detail from one sampling period to another under the same overall meteorological conditions. Therefore, predictions of even a perfect model will differ from observed values if the averaging time is not long enough. This expected deviation of observations from predictions gives rise to the "inherent uncertainty".

Some studies have attempted to estimate the expected deviation of observed concentrations of pollutants from predicted ensemble means. For instance, Venkatram (1979) showed that the inherent uncertainty is proportional to the time scale (characteristic time) controlling dispersion in the plume and to the ratio of the instantaneous peak and mean concentrations and is inversely proportional to the averaging time. On the other hand, Weil *et al.* (1992) recognized that the inherent uncertainty is difficult to estimate in flows in the atmospheric boundary layer (ABL). However, they attempted to separate the model error from the variability arising from the stochastic nature of pollutant dispersion in a turbulent flow in order to evaluate the model physics.

Laboratory experiments have provided important data on turbulence-driven pollutant dispersion and are the basis of the most advanced models (Venkatram and

Wyngaard, 1988). In Chapter 2 of this dissertation we study the relationship between inherent uncertainty in atmospheric and laboratory flows. We use this relationship to infer the expected deviation of observed concentrations of pollutants from model predicted means in the ABL from laboratory-derived inherent uncertainties (Stein and Wyngaard, 2001).

Dispersion models are only used to obtain concentration fields of inert gases, and their domain covers just a few kilometers downwind of a pollution source. These models are unable to simulate the formation of secondary pollutants over a scale bigger than tens of kilometers. Therefore, we need to increase the level of simulation complexity and include the interactions between meteorological processes and gas-phase photochemical reactions to model secondary contaminant formation such as ozone (O_3) in the lower troposphere.

Ozone is a reactive oxidant gas produced in trace amounts in the Earth's atmosphere. In the troposphere this gas is formed when an atom of oxygen, usually produced by solar photodissociation of nitrogen dioxide, combines with molecular oxygen. Elevated ozone concentrations have been observed over different geographical regions, particularly in densely populated urban, suburban, and even in rural areas (Trainer *et al.*, 1991). Part of the complexity of the tropospheric ozone problem comes from the fact that O_3, more so than most other pollutants, shows a great variability depending on meteorological conditions. Ozone is photochemically produced, so on cloudy days and at nighttime its production is minimized. In addition, there is a strong correlation between the rate of O_3 production and temperature. For the most part,

significant amounts of ozone are formed when temperatures are high (Cardelino and Chameides, 1990).

Over the last two decades considerable effort has been devoted to regulating and reducing the levels of tropospheric ozone in various regions of the world. Exposure to high levels of O_3 can cause damage to people, animals and vegetation. Clinical studies have found a significant relationship between ozone exposure and several acute respiratory conditions, including coughing, shortness of breath, nose and throat irritation, and chest discomfort (Brunekreef *et al.*, 1995 and references therein). Due to the negative health effects associated with exposure to high ozone concentrations, it is important to develop tools that predict and warn the ozone-sensitive population of pollution events. Toward that end, a three-dimensional hybrid (Lagrangian-Eulerian) model has been applied to forecast summertime ozone concentrations.

The Hybrid Single-Particle Lagrangian Integrated Trajectories with a generalized non-linear Chemistry Module (HY-SPLIT CheM) model has been developed to calculate the spatial and temporal distribution of different chemical species in the troposphere over a regional scale (Stein *et al.*, 2000). The simulation accounts for the advection, dispersion, chemical transformation, and deposition of the different pollutants. In Chapter 3 we present a description of the model implementation procedures to forecast ozone concentrations over the Northeastern United States. Also, the ability of HY-SPLIT CheM to simulate ozone mixing ratios is evaluated by comparing calculated summertime ozone mixing ratios against measured values.

Finally, the study of the formation of aerosol particles, specifically sulfate aerosols, involves a complicated coupling between not only gas-phase chemical reactions, such as in the case of O_3, but also between aqueous-phase photochemical and meteorological processes within the simulation framework. In consequence, the third study in this dissertation involves modeling and measurements of aerosol sulfate and the development of indicators of sulfate sensitivity to changes in nitrogen oxides and hydrocarbons source strengths.

Sulfate (SO_4^{2-}) is the dominant inorganic constituent of ambient aerosol particles with diameters of 2.5 μm or less (i.e., $PM_{2.5}$) in the eastern United States (Hidy *et al*., 2000). High levels of aerosol particles pose possible health hazards and impact the environment in a variety of ways. Indeed, numerous epidemiological studies have established a relationship between the abundance of ambient fine particles and mortality (Dab *et al*., 2001; Brenekreef *et al*., 1995). Consequently, in 1997, the Environmental Protection Agency (EPA) proposed a modification of the National Ambient Air-Quality Standard (NAAQS) to include $PM_{2.5}$. This revised standard was set at 15 μg m^{-3}, annual mean, and 65 μg m^{-3} for a 24-hour average (EPA, 1996a). On the other hand, tropospheric sulfate particles affect regional and global climates by scattering radiation directly (Charlson *et al*., 1991) and indirectly by altering the scattering characteristics of clouds (Twomey *et al*., 1984). In addition, their hygroscopic nature permits sulfate aerosols to reduce visibility at high relative humidities (Waggoner *et al*., 1981; Malm *et al*., 1994) and to affect the formation of photochemical smog by enhancing actinic fluxes (Dickerson *et al*., 1997). The deposition of sulfate can affect the environment in other

ways, such as by elevating acidity levels in surface waters and soils. Acidic deposition causes the leaching and removal of some nutrients from tree foliage, changes soil-water and surface-water chemistry, and may contribute to adverse biological effects in sensitive lakes, streams, and forests (NAPAP, 1993).

Understanding the atmospheric processes that lead to the formation of sulfate is crucial to the development of effective policies to control their formation, deposition and potential damage to human health and aquatic and terrestrial ecosystems. The combustion of fossil fuels containing sulfur leads to emissions of sulfur dioxide (SO_2), a gaseous compound that can be chemically transformed (oxidized) into sulfuric acid (H_2SO_4) once it is released into the atmosphere. The oxidation step can take place either in the gas phase or within liquid cloud droplets, but either way the resulting sulfate resides almost exclusively in the condensed phase. Aqueous-phase H_2SO_4 dissociates into hydronium (H_3O^+) and sulfate (SO_4^{2-}) ions that are subsequently deposited at the Earth's surface, either in precipitation or as "dry" particles.

Theoretical studies (e.g., McHenry and Dennis, 1994; Karamchandani and Venkatram, 1992; Shin and Carmichael, 1992), as well as atmospheric measurements (Dutkiewicz *et. al.*, 1995; Van Valin *et. al.*, 1991), have been used to determine the relative importance of the different pathways by which SO_2 is oxidized to SO_4^{2-} and the various oxidants involved. Calvert *et al.* (1978) and Eggleton and Cox (1978) showed that the hydroxyl radical (OH) is the primary clear-air oxidant for SO_2, while Stockwell and Calvert (1983) confirmed that this pathway does not alter the abundance of odd-hydrogen species. McHenry and Dennis (1994) estimated that the production of sulfate

in clear-air under summertime conditions in eastern North America accounts for 30-40% of the total ambient sulfate budget. By contrast, oxidation of SO_2 in clouds has been estimated to contribute over 50% of the sulfate in summertime rains (Karamchandani and Venkatram, 1992), the primary aqueous-phase oxidant most likely being hydrogen peroxide (H_2O_2) in this region (Penkett *et al.*, 1979; McHenry and Dennis, 1994).

Traditionally, strategies to control sulfate formation have been focused on the response of SO_4^{2-} to reductions in sulfur dioxide (SO_2) emissions (Misra *et al.*, 1989; Rolph *et al.*, 1992; Mathur *et al.*, 1992; Shin and Carmichael, 1992). Many aspects of this relationship have been extensively covered throughout the literature. For instance, Kleinman and Daum (1991) addressed the possibility of a nonlinear response in SO_4^{2-} production to changes in SO_2 levels. Such a nonlinear behavior may arise when more SO_2 exists in the air than can be oxidized by the available oxidants. Stockwell (1994a), on the other hand, studied the impact of changes in SO_2 concentration on the oxidant levels themselves and found that the gas-phase SO_2 oxidation mechanism significantly enhances H_2O_2 production rates, a process that tends to offset the nonlinearity arising from oxidant limitations.

Much less attention has been devoted to assessing the effects on sulfate formation arising from changes in emissions of volatile organic compounds (VOC) and nitrogen oxides (NO_x), the chemical families largely responsible for the generation of the tropospheric oxidants needed to transform SO_2 to SO_4^{2-}. The response of ambient sulfate to reductions in NO_x and VOC emissions depends in part on the resulting changes in oxidant levels and the competition that naturally exists between in-cloud and clear-air

SO_2 oxidation. Coupling of the different chemical families leads to complex and potentially non-linear behavior with non-intuitive consequences.

We attempt to gain insight into the relationship between the oxidants of SO_2 and their precursors (NO_x and VOC) and therefore into possible impacts on SO_4^{2-} formation. Toward this end, Chapter 4 presents a first case study in which a large amount of ambient SO_4^{2-} was measured in the air prior to a heavy rain event loaded with high concentrations of H_3O^+ and SO_4^{2-} over central Pennsylvania. This case study reveals that huge acid deposition events are possible even after the major reductions in SO_2 emissions that have occurred as a consequence of the Clean Air Act Amendments of 1990 (Lynch *et al.*, 2000). Meteorological and chemical modeling has been performed to identify the likely processes by which the ambient SO_4^{2-} was formed.

Chapter 5 presents a theoretical analysis of sulfate-formation pathways to establish the effectiveness of VOC or NO_x controls in decreasing SO_4^{2-} abundance. Then, we introduce a second case study in which photochemical species are simulated with a three-dimensional Eulerian model (MODELS-3) that covers the eastern United States. Following the approach of Sillman (1995), we use a set of "indicator species" to determine thresholds for ozone (O_3) -NO_x-VOC- sensitivity that can be evaluated against literature values and gain confidence in the model predictions. Finally, by extension of the concept to sulfate, the threshold concentrations of the indicator species for ambient SO_4^{2-}-VOC-NO_x sensitivity are derived (Stein and Lamb, 2001).

Chapter 2

DISPERSION MODELING AND THE EVALUATION OF INHERENT UNCERTAINTY

Atmospheric dispersion models are widely used to estimate the impact of non-reactive pollutant releases into the atmosphere. Most such models predict the ensemble-average concentration field, the average over a large collection of releases under similar externally imposed conditions. But the stochastic nature of pollutant dispersion in the atmospheric boundary layer (ABL) makes pollutant concentrations vary greatly from one sampling period to another under the same meteorological conditions. Therefore, if the sampling time is not sufficiently long, the values predicted by even a perfect model will inevitably differ from mean values measured in the atmosphere. The ratio of their root mean square (rms) difference and the ensemble-average concentration is called the inherent uncertainty. This work investigates the relationship between inherent uncertainty in laboratory and ABL flows.

Approach

We represent $\tilde{c}(\boldsymbol{x},t)$, the concentration at point $\boldsymbol{x}$ and time t, as the sum of ensemble-mean and fluctuating parts:

$$\tilde{c}(\boldsymbol{x},t) = C(\boldsymbol{x},t) + c(\boldsymbol{x},t). \tag{2-1}$$

The ensemble-average concentration C is defined as

$$C = \lim_{N\to\infty} \frac{1}{N} \sum_{\alpha=1}^{N} \tilde{c}(\boldsymbol{x},t;\alpha), \tag{2-2}$$

where α is the realization number of the experiment. In practice we typically estimate the ensemble mean by averaging over time. We denote this finite-time mean as C^T:

$$C^T = \frac{1}{T}\int_0^T \tilde{c}(t)dt. \tag{2-3}$$

For finite averaging time C^T will differ in general from C. A measure of the difference between a finite-time average and the ensemble average in statistically steady conditions is the variance of their difference, which for a general function $f(t)$ is given by (Tennekes and Lumley, 1972)

$$\overline{(f^T - \bar{f})^2} = \frac{2\overline{(f - \bar{f})^2}}{T}\int_0^T (1 - \frac{t}{T})\rho(t)dt, \tag{2-4}$$

where $\overline{(f - \bar{f})^2}$ is the variance of $f(t)$ and $\rho(t)$ is the auto-correlation function of $f(t)$. The integral scale τ of $f(t)$, defined as

$$\int_0^\infty \rho(t)dt = \tau, \tag{2-5}$$

is a measure of the "memory time" of $f(t)$. For averaging time T much longer than τ we can approximate (2-4) as

$$\overline{(f^T - \bar{f})^2} \approx \frac{2\overline{(f - \bar{f})^2}}{T}\tau. \tag{2-6}$$

Equation (2-6) shows that the larger the variability in a signal *f(t)*, the larger its integral scale, or the smaller the averaging time, the lower the accuracy of using f^T as an estimate of the ensemble mean $\bar{f}$.

Let us consider two sets of geometrically similar experiments carried out under the same stability conditions in the laboratory (*lab*) and in the atmosphere (*atm*). Let us define $\varepsilon = \left[\overline{(f^T - \bar{f})^2}\right]^{1/2} \Big/ \bar{f}$ as the inherent uncertainty, so that from (2-6) with $f = \tilde{c}$

$$\varepsilon^2 \approx \frac{2\overline{c^2}\tau}{C^2 T}. \qquad (2\text{-}7)$$

The ratio of the inherent uncertainties associated with the atmospheric and the laboratory flows is

$$\frac{\varepsilon_{atm}}{\varepsilon_{lab}} \approx \left[\frac{\overline{c^2}_{atm} C_{lab}^2 T_{lab} \tau_{atm}}{\overline{c^2}_{lab} C_{atm}^2 T_{atm} \tau_{lab}}\right]^{1/2}. \qquad (2\text{-}8)$$

The gross structure of turbulent flows of the same geometry is observed to be similar over a very wide range of Reynolds numbers, providing these Reynolds numbers are sufficiently large and "…the boundary conditions of the flow system can be expressed non-dimensionally in terms of a linear dimension M and a velocity U_1… If such a flow is investigated, it is usual to find that most mean-value functions, when expressed non-dimensionally in terms of M and U_1, are functions of the non-dimensional space coordinates x_1/M, x_2/M, x_3/M, which do not depend on the Reynolds number…" (Townsend, 1956). This makes it possible to model atmospheric boundary-layer flows in

the laboratory (Snyder, 1981). Making use of this concept, better known as Reynolds-number similarity (Tennekes and Lumley, 1972), we can assume that

$$\frac{\overline{c^2}_{atm}}{C^2_{atm}} \approx \frac{\overline{c^2}_{lab}}{C^2_{lab}}. \tag{2-9}$$

This assumption constitutes the basis for the design of a laboratory model of an atmospheric diffusion problem. There are some situations in which the source features, such as stack diameter, have an influence on the ratio of the variance to the ensemble mean, for instance when atmospheric measurements are taken very close to the stack. Under these conditions, the source characteristics should be taken into account when designing a geometrically similar laboratory experiment. If the Reynolds number in the laboratory stack is large enough, however, (2-9) should still hold.

Replacing (2-9) into (2-8), we obtain

$$\frac{\varepsilon_{atm}}{\varepsilon_{lab}} \approx \left[\frac{T_{lab}\tau_{atm}}{T_{atm}\tau_{lab}}\right]^{1/2}. \tag{2-10}$$

Furthermore, since the integral scale is determined by the energy-containing parts of the flow, which by hypothesis are Reynolds-number similar, we can write

$$\frac{\tau_{atm}}{\tau_{lab}} \approx \frac{l_{atm}/U_{atm}}{l_{lab}/U_{lab}}, \tag{2-11}$$

where l and U are the characteristic length and velocity scales of the flow. From (2-11), then (2-10) becomes

$$\frac{\varepsilon_{atm}}{\varepsilon_{lab}} \approx \left[\frac{T_{lab}l_{atm}U_{lab}}{T_{atm}l_{lab}U_{atm}}\right]^{1/2}. \tag{2-12}$$

Equation (2-12) has profound implications for the relative inherent uncertainties and averaging times in atmospheric and laboratory flows. If, for example, $l_{atm}/l_{lab} \approx 10^4$ and $U_{atm}/U_{lab} \approx 10^2$, which are characteristic values for the ABL and water-tank simulations of Willis and Deardorff (1976), then (2-12) gives

$$\frac{\varepsilon_{atm}}{\varepsilon_{lab}} \approx 10\left[\frac{T_{lab}}{T_{atm}}\right]^{1/2}. \qquad (2\text{-}13)$$

For the same averaging time ($T_{atm}=T_{lab}$) this says the inherent uncertainty in the atmospheric flow is 10 times that in the laboratory flow. For the same inherent uncertainty, the averaging time required for the atmospheric measurements is 100 times that in the lab. Figure 1 summarizes these findings.

We can illustrate the implications of (2-12) through a practical example based on measurements of the dispersion of particulate tracers in a convective water tank (Willis and Deardorff, 1976). Details of the experimental design can be found there. The particles are released from an instantaneous line source that, after assuming that Taylor's hypothesis holds, can be mathematically transformed to represent a continuous point source. Figure 2 shows mean concentrations measured in a given *y*-*z* plane, located at a dimensionless distance $\boldsymbol{X}$=0.68 downwind of the simulated point source in the laboratory model of a convective boundary layer. This dimensionless distance is defined by $\boldsymbol{X}=(x/z_i)(w_*/U)$, where x is the coordinate aligned with the mean wind U, z_i represents the mixed layer depth and w_* is the convective velocity scale, $w_*=(g\alpha Q_0 z_i)^{1/3}$, where α is the

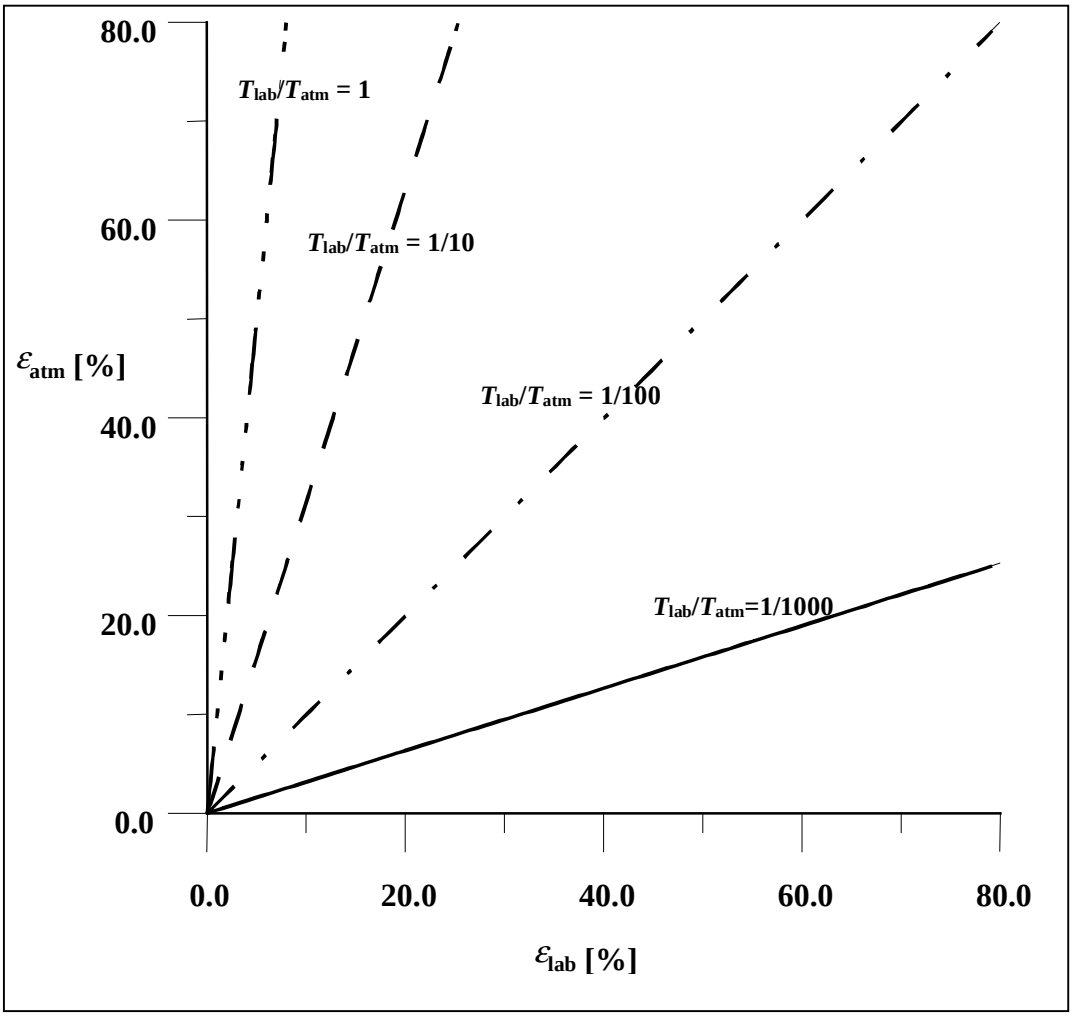

Figure 1: Calculated inherent uncertainty in the atmospheric flow as a function of the inherent uncertainty in the laboratory flow for fixed ratios of averaging times corresponding to a length scale ratio of 10^4 and a mean wind ratio of 10^2.

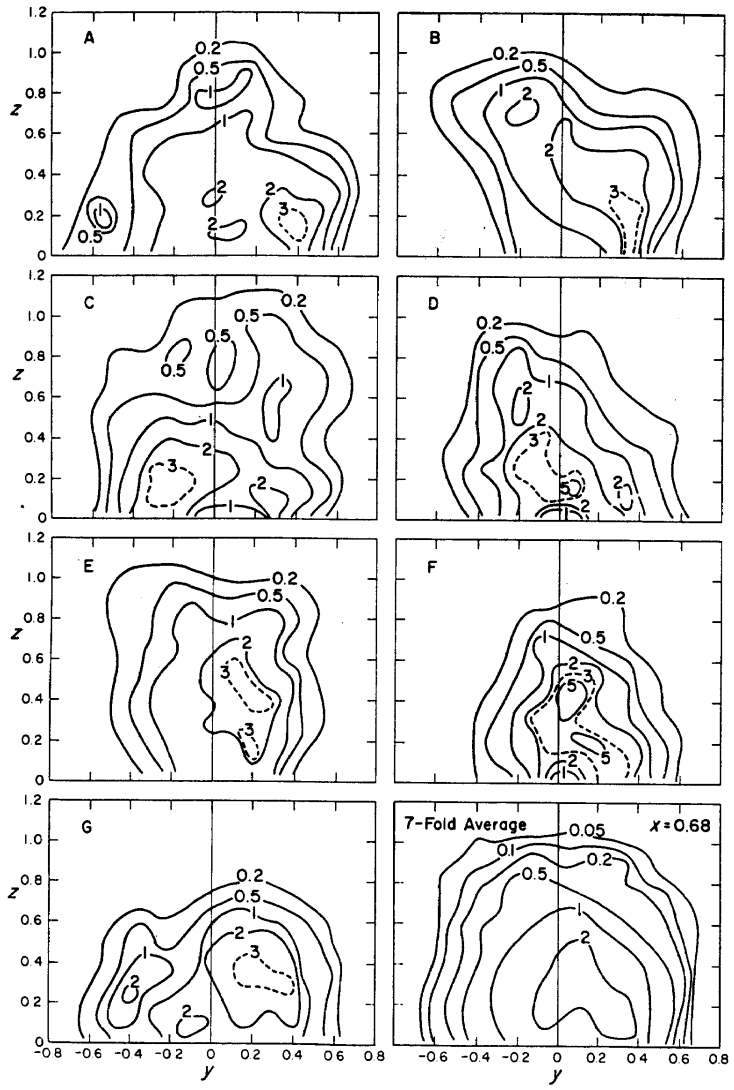

Figure 2: Concentration contours for laboratory simulation of diffusion from a continuous point source in a convective ABL (From Willis and Deardorff, 1976). The seven plots labeled A-G are 20-30-s averaged concentrations (C^T) and the final plot is the average of these seven.

coefficient of thermal expansion and Q_0 is the kinematic heat flux near the surface. The seven plots in Figure 2 labeled A-G are time averages (C^T) and the final plot is the average of these seven. Because these concentration measurements were taken perpendicularly to the instantaneous line source, they integrate the effect of turbulent diffusion along the release line of length $4z_i$. Consequently, Willis and Deardorff (1976) estimated that their measurements represent a concentration field downwind of a continuous release from a point source with an equivalent sampling time of $4z_i/U$, which corresponds to a 20-30 s averaging time.

An example

From Figure 2 we estimated $\overline{(C^T - C)^2}$ over the *y*-*z* plane, approximating the ensemble average, *C*, as the average over the seven runs. The resulting inherent uncertainty $\varepsilon = \left[\overline{(C^T - C)^2}\right]^{1/2} / C$ estimates from (2-12) are shown in Figure 3. The ε values are mostly higher than 50% and increase toward the edges of the measurement field. These ε values are themselves necessarily uncertain, of course, because they were determined from an ensemble with only seven realizations. With (2-13) we can estimate the corresponding inherent uncertainty and averaging time for the atmospheric case. To achieve the same inherent uncertainty in the atmosphere and in the laboratory ($\varepsilon_{atm}=\varepsilon_{lab}$) given that $T_{lab} \approx$ 20-30 s, we find that $T_{atm} \approx 100\ T_{lab} \approx 1$ h. If we would like to achieve a 10% inherent uncertainty in the atmosphere ($\varepsilon_{atm}=0.1$) with $\varepsilon_{lab}=0.5$, this indicates that the required averaging time is approximately 1 day. This is only a rough estimate, given the uncertainty of our laboratory ε value. Even if that uncertainty were as large as 50%,

however, our estimate gives startling indications of the large inherent uncertainty that can exist in the typical one-hour-average concentrations in ABL diffusion problems.

The models routinely used in atmospheric dispersion of pollutants are often claimed to predict 1-hour average concentrations. We showed that the inherent uncertainty of one-hour averages can be high in dispersion problems in the ABL. Furthermore, the averaging times required for convergence of the time average to the ensemble average predicted by the models can be large and non-stationarity effects can render them difficult to achieve.

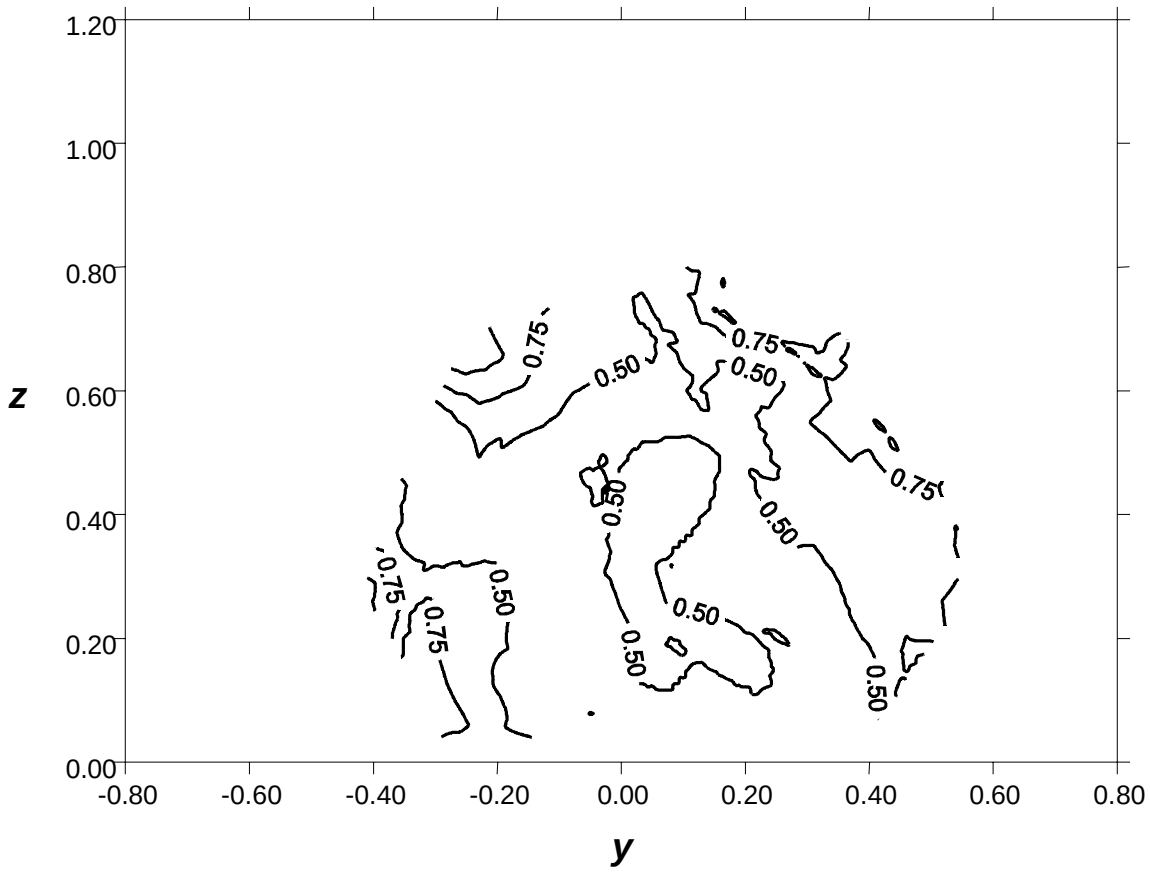

Figure 3: Calculated inherent uncertainty contours for the data of Figure 2.

Chapter 3

OZONE FORECASTING FOR NORTHEASTERN UNITED STATES USING A HYBRID (LAGRANGIAN-EULERIAN) PHOTOCHEMICAL MODEL

As discussed in the previous Chapter, dispersion models that predict ensemble-averaged concentrations of non-reactive chemical species, e.g. Gaussian-type models, would exhibit high inherent uncertainties for 1-h averages. One of the primary causes for these elevated inherent uncertainties is that Gaussian models do not fully represent a time-varying concentration field because they correspond to an average over a large collection of pollutant releases under similar externally imposed conditions. Therefore, including time-dependent concentrations would in principle diminish this uncertainty. Moreover, Gaussian models have serious limitations for simulating the formation of secondary pollutants. As a consequence, we next describe the use of a time-dependent photochemical model that simulates the formation of tropospheric ozone on the regional scale.

Model description

Overview

The Hybrid Single-Particle Lagrangian Integrated Trajectories with a generalized non-linear Chemistry Module (HY-SPLIT CheM) model has been developed to calculate

the spatial and temporal distribution of tropospheric ozone over a regional scale (Stein *et al.*, 2000). The HY-SPLIT CheM model assumes that the entire pollutant mass at each emission source is uniformly distributed among a number of "particles", each of which may be thought of as a capsule containing the various chemical species. These particles are advected, dispersed, and deposited throughout the simulation domain. The concentration of each chemical species within a cell is calculated by dividing the sum of the particle masses of a particular chemical compound by the volume of the corresponding concentration grid cell in which the particles reside, so uniform mixing inside each cell is assumed. The time evolution of the system due to chemical interactions is then computed by solving a stiff set of differential equations that represent the chemical changes taking place within each cell. The resulting concentrations are then utilized to calculate the new masses of the chemical species back to the particles within the cell.

Emissions

The VOC, carbon monoxide (CO) and NO_x emissions are based on the 1995-1996 Ozone Transport Assessment Group (OTAG) emissions inventory (EPA, 1999a). This inventory has a 1/9x1/6 degrees resolution and is subsequently averaged over a 1/2x1/2 degrees emission grid. All point, mobile and non-mobile emissions are included, with no distinction made in the heights of emissions from point sources. VOC emissions represent all non-methane hydrocarbons. Methane (CH_4), which is therefore not included in the emissions, is assumed to be uniformly distributed at a constant mixing ratio of 1.7 ppm. Isoprene emissions are calculated as a function of temperature, insolation, and land

use (Jacob *et al.*, 1993). The number of moles of each chemical species assigned to each "particle" is based on the given emission rate multiplied by the emission time interval. Pollutant emissions are simulated by releasing several particles at the center of each emission grid every time step, with the number of particles released from each emission cell being fixed. The total number of particles released per hour in the whole domain is a given parameter. The model divides the total number of particles by the number of emission cells to obtain the number of particles released in each cell every time step.

Transport and dispersion

Each particle is subjected to advection and dispersion by the transport module. The HY-SPLIT_4 model used in this study as the transport-dispersion module is a hybrid between Eulerian and Lagrangian approaches. The foundation of the model resides in the fact that advection and dispersion are computed following a Lagrangian particle. The advection of each particle is computed independently, so once the basic meteorological data have been processed and interpolated to the internal model grid, trajectories can be calculated (Rolph *et al.*, 1993).

The meteorological data used by this model are obtained as output fields from a variety of different meteorological models (e.g., National Center for Environmental Prediction (NCEP) ETA model). The horizontal grid system used by HY-SPLIT_4 is designed to be identical to that of the meteorological data. In order to allow the use of different meteorological data sources for input, the vertical profiles of the meteorological

data at each horizontal grid point are linearly interpolated to a terrain-following (σ) coordinate system. Namely,

$$\sigma = 1 - z/Z_{top} \tag{3-1}$$

where z is the height expressed relative to the terrain and Z_{top} is the top of the HY-SPLIT_4 coordinate system. The advection is determined from the average of the three-dimensional velocity vectors, $V(P,t)$, for the initial position $P(t)$ and the first-guess position $P'(t+\Delta t)$. The velocity vectors are linearly interpolated in both space and time. The first-guess position is

$$P'(t+\Delta t) = P(t) + V(P,t)\,\Delta t \tag{3-2}$$

and the final position is given by

$$P(t+\Delta t) = P(t) + 0.5\,[V(P,t) + V(P',t+\Delta t)]\,\Delta t \tag{3-3}$$

The integration time step (Δt) can vary during the simulation. It is computed from the requirement that the advection distance per time-step should be less than the grid spacing. This integration method is known as the *improved Euler-Cauchy method* (Kreyszig, 1967, p.88).

The concentration of the i^{th} species within the concentration cell located at position x, y, and z, is calculated by

$$C_{i,j,x,y,z} = \frac{1}{\Delta x \Delta y \Delta z} \sum_{j=1}^{N_{x,y,z}} m_{i,j,x_p,y_p,z_p} \quad , \tag{3-4}$$

where $m_{i,j,xp,yp,zp}$ is the number of moles of the i^{th} chemical species corresponding to the j^{th} particle, which is located at x_p, y_p, z_p within the cell ($x \pm \Delta x/2$, $y \pm \Delta y/2$, and $z \pm \Delta z/2$), and where $N_{x,y,z}$ is the total number of particles within the cell. The size of the concentration cell is specified by the dimensions Δx, Δy, and Δz. It should be noticed that Equation (3-4) represents the transition from the Lagrangian to the Eulerian approach.

The dimensions (horizontal and vertical) of the concentration grid can differ from the transport-dispersion (meteorological) grid. For instance, the advection and dispersion of the particles can be calculated using meteorological data interpolated to 20 vertical meteorological grid layers with a horizontal resolution of 180 km, whereas the concentrations of the chemical species can be computed using one or two vertical layers and a horizontal resolution of 50 km.

Gas-phase chemistry

Once the concentrations of all species have been calculated at each cell of the concentration grid the chemical evolution of the system is computed for the corresponding time step. When the density of the air can be assumed to be constant within each grid cell, the concentrations are converted to mixing ratios (i.e., ppm) using the following expression

$$y_{i,x,y,z} = \frac{RT_{x,y,z}}{P_{x,y,z}} \times C_{i,x,y,z} \quad , \qquad (3\text{-}5)$$

where $y_{i,x,y,z}$ is the mixing ratio of the i^{th} species corresponding to the concentration grid located at grid position x, y, and z, R is the ideal gas constant, $T_{x,y,z}$ is the temperature, and $P_{x,y,z}$ is the pressure.

The gas-phase chemistry module used in this work assumes uniform mixing of individual constituents within a concentration grid. The chemistry is thus treated exactly as in a well-mixed reactor. This idea is expressed mathematically as

$$\frac{dy_{i,x,y,z}}{dt} = \frac{(Q_{i,x,y,z} - L_{i,x,y,z})}{N} \quad , \tag{3-6}$$

where N is the total atmospheric number density, $Q_{i,x,y,z}$ is the rate of production and $L_{i,x,y,z}$ is the rate of loss of the i^{th} species within the concentration grid located in the position x, y, and z. This system of stiff ordinary differential equations is solved by the Gear's method (Gear, 1971; Press *et al.* 1992), as modified by Spellmann and Hindmarsh (1975).

The Carbon Bond Mechanism IV (CBM-IV) (Gery *et al*., 1989) was used to describe the gas-phase chemical processes that occur within the concentration grids. This chemical scheme utilizes the carbon-bond approach for the lumping of organic species. Under this approach, organic species are disaggregated according to their bond type (for example, as carbon single bonds, carbon double bonds, or carbonyl bonds). The CBM-IV contains over 80 reactions and more than 30 chemical species. The photolysis rate constants needed to calculate the chemical transformations are computed as a function of the solar zenith angle, cloud cover, and chemical species for each concentration grid cell.

Redistribution of mass

After the chemical transformations have been calculated, the resulting concentrations are then used to update the number of moles of each chemical compound in every particle. This redistribution step constitutes the transition from the Eulerian back

to the Lagrangian framework. Although many possibilities exist for computing the number of moles in the particles (Chock and Winkler, 1994), the calculation should be simple, reliable, and computationally efficient. HY-SPLIT CheM accomplishes this by implementing the following procedure:

If $C_{i,x,y,z}(t + \Delta t) > C_{i,x,y,z}(t)$, then for those particles that already have an initial number of moles of a given compound (*i*),

$$m_{i,j,x_p,y_p,z_p}(t+\Delta t) = (1-\frac{n_{i,x,y,z}}{N_{x,y,z}}) \times \frac{C_{i,x,y,z}(t+\Delta t)}{C_{i,x,y,z}(t)} \times m_{i,j,x_p,y_p,z_p}(t) \quad , \qquad (3\text{-}7)$$

where $n_{i,x,y,z}$ and $N_{x,y,z}$ are the number of particles of the i^{th} species with zero moles and the total number of particles within the concentration grid located at *x*, *y*, and *z*, respectively. If a particle began with zero moles for a certain chemical species, as may occur for the formation of secondary compounds, then the corresponding number of moles are distributed equally among those particles within the same concentration grid cell. Mathematically,

$$m_{i,j,x_p,y_p,z_p}(t+\Delta t) = \frac{1}{N_{x,y,z}} \times C_{i,x,y,z}(t+\Delta t) \times \Delta x \Delta y \Delta z \, . \qquad (3\text{-}8)$$

On the other hand, if $C_{i,x,y,z}(t + \Delta t) \leq C_{i,x,y,z}(t)$ then the mass is only redistributed among those particles that already had a number of moles different from zero. Namely,

$$m_{i,j,x_p,y_p,z_p}(t+\Delta t) = \frac{C_{i,x,y,z}(t+\Delta t)}{C_{i,x,y,z}(t)} \times m_{i,j,x_p,y_p,z_p}(t) \, . \qquad (3\text{-}9)$$

This kind of distribution ensures that particles with zero number of moles of a given chemical species will acquire that species only if there is a net production of that

chemical compound. For instance, particles released during the night hours will be assigned zero moles of ozone reflecting the fact that there is no net production for this compound. Only when the net ozone production is greater than zero do these particles receive their corresponding number of moles for ozone.

Once the redistribution has been performed, advection and dispersion take place again, followed by the computation of the chemical transformations and dry deposition for the next time step. New particles are released every time step from the sources to simulate fresh emissions of pollutants.

Dry deposition

Dry deposition is considered whenever the particle position is within the surface layer, defined as the second meteorological data level (usually around 75 m). Dry removal is assumed to be a first-order process, so the rate coefficient $k_{d,i}$ is calculated by

$$k_{d,i} = \frac{V_{d,i}}{\Delta z_p} \quad , \tag{3-10}$$

where $V_{d,i}$ is the deposition velocity for the i^{th} species, and Δz_p is the particle vertical position. The deposition velocity can be calculated by the resistance method (Draxler and Hess, 1997) or alternatively it can be explicitly defined. If the resistance method is used to calculate the deposition velocity, then $V_{d,i}$ is given by

$$V_{d,i} = [R_a + R_b + R_c]^{-1} \ , \tag{3-11}$$

where the subscripts for the resistances R represent the atmospheric layer or aerodynamic resistance (a), the quasi-laminar sub-layer or laminar boundary layer resistance (b), and

the canopy layer or surface resistance (*c*), which represents the collective resistance of various surfaces (Hertel *et al.*, 1995). The resistance components depend upon meteorological conditions as well as the properties of the surface (Wesely and Hicks, 1977). More detail on each of the resistance components can be found in Draxler and Hess (1997). For the purposes of this work we explicitly provided the dry deposition velocities for the chemical species as given by Hertel *et al.* (1995).

Model Implementation

The simulation domain extends over the latitudes 35.5 ^{o}N to 45.5 ^{o}N and the longitudes 72.5 ^{o}W to 87.5 ^{o}W. This size ensures the inclusion of sources that influence O_3 formation in Northeastern United States. Back-trajectory calculations provide the necessary information to locate such sources and set the extension of the simulation domain. The dimensions of each concentration cell are 1/2x1/2 degrees. Three vertical layers are used, one from the surface to 500 m, the second from 500 m to 2,000 m and the third one from 2,000 m to 6,000 m. A total of 5,000 particles are released from all the sources at each simulation hour.

Transport, dispersion, and biogenic emissions are computed using meteorological fields from the National Oceanic and Atmospheric Administration (NOAA) National Center for Environmental Prediction (NCEP) ETA model with a resolution of 40 km in the horizontal, and 25 mb in the vertical, based upon the 0000 UTC forecast. Calculations for each day start with all the pollutant particles that are on the domain at the initialization time as computed from the previous day simulation. Pollutant particles may

accumulate for up to 72 hours before termination. However most particles are advected off the model domain prior to reaching their age limit.

Model Performance

Summertime ozone mixing ratios are calculated and compared against measured values throughout the Northeastern United States. The entire month of July 1999 has been chosen for testing the performance of HY-SPLIT CheM. A wide range of ozone concentrations was measured and a considerable variety of synoptic-scale meteorological patterns, that could influence the spatial O_3 distribution, were observed over the period of time under study.

Measurements of hourly averaged ozone mixing ratios were obtained from the Aerometric Information Retrieval System (AIRS). The AIRS is a computer-based repository of information about airborne pollution in the United States and various World Health Organization member countries (AIRSweb, 1998). A total of 350 measurement stations distributed throughout the Northeastern United States was chosen to make the model comparison.

In order to spatially pair the modeled and the measured ozone concentrations a bi-linear horizontal interpolation was performed over the simulated values to the corresponding monitor location. It should be noted that the model results represent an average over a 50x50x0.5 km^3 cell, whereas the observations are point measurements taken at fixed locations. Therefore, caution should be exercised when comparing modeled and measured ozone concentrations. Some situations occur when a considerable portion of the bias between modeled and observed O_3 concentrations can be explained, for

instance, by the coarse vertical resolution of the concentration grid (Byun and Dennis, 1995). In this particular study (Stein *et al.*, 2000) we observed that at some sites there is a lag in the peak modeled ozone concentration that can be attributed to the coarse grid size. At sunset, when the nocturnal inversion forms, the O_3 concentration shows a strong vertical gradient near the surface due to the depletion of O_3 by dry deposition. However, the model does not completely capture this feature due to its coarse vertical resolution. Hence the ozone concentration continues to build up in the lower layer. On the other hand, during the day, the O_3 is well mixed throughout the planetary boundary layer (PBL), and the near surface concentrations should be representative of the PBL as a whole. As a consequence we only use the maximum 1-hour model interpolated and observed ozone concentrations from 1400 UTC to 2000 UTC to perform the statistical analysis in order to reduce the influence of these phenomena.

The model was evaluated by making use of the raw bias, raw gross error, and coefficient of determination (r^2) between observed and modeled ozone as statistical performance measures (McHenry *et al.*, 2000). Figure 4 shows the raw bias as a function of simulation day. HY-SPLIT CheM predicts the 1-hour O_3 peak with a daily raw bias of ±20 ppb (Figure 4). The model tends to underpredict the measured data slightly. One of the possible causes of these simulated low concentrations can be related to the model's coarse grid resolution. In the simulation, the particles are released from the sources into grids of 500 m height, producing an instantaneous dilution that is reflected in the low ozone concentrations. Also an insufficient number of particles within the model domain could partially explain the underprediction. For instance, some particles could miss

certain grids and therefore would not contribute to a concentration enhancement. Moreover, the 1995-1996 OTAG inventory may represent an underestimate of the 1999 emissions (McHenry *et al*, 2000), further explaining the underestimation in O_3 and its precursors. On the other hand, Figure 5 shows that the raw gross errors are generally below 30 ppb.

Figure 6 shows the variation of the coefficient of determination throughout the forecasting period. This coefficient reflects the ability of the model to predict the geographical distribution of the concentration of ozone. In general, the model captures the major geographic ozone features for the high-ozone cases, namely, July 15-19, 22-25, and 27-31. On the other hand, low r^2 are generally associated with a poor performance of the meteorological model, as in the cases of July 1-2, 11 and 20-21, where the photochemical model tends to misplace the ozone concentration spatial features. A comparison between the Eta Data Assimilation System (EDAS) (http://www.arl.noaa.gov/ready/amet.html) and the Eta forecast meteorological data reveals that there was a misplacement of the cloud coverage fields, which in turn influenced the downward short wave irradiance field. This discrepancy between the irradiance fields further affected the photolysis rate constants, further explaining the low r^2 between the observed and measured ozone mixing ratios. However, a coarse photochemical model resolution, as well as errors in the emissions inventories, may also contribute to the deterioration of the performance of the simulation.

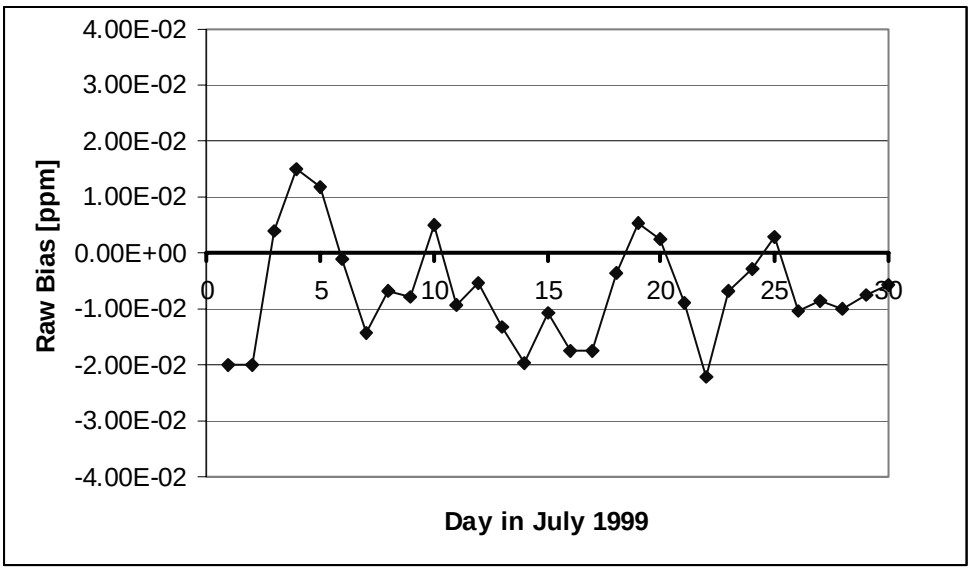

Figure 4: Raw bias as a function of simulation day. Raw bias: $\frac{1}{N}\sum_{i=1}^{N}[X_{p,i}(t) - X_{o,i}(t)]$, where X_p is the modeled and X_o is the measured mixing ratio.

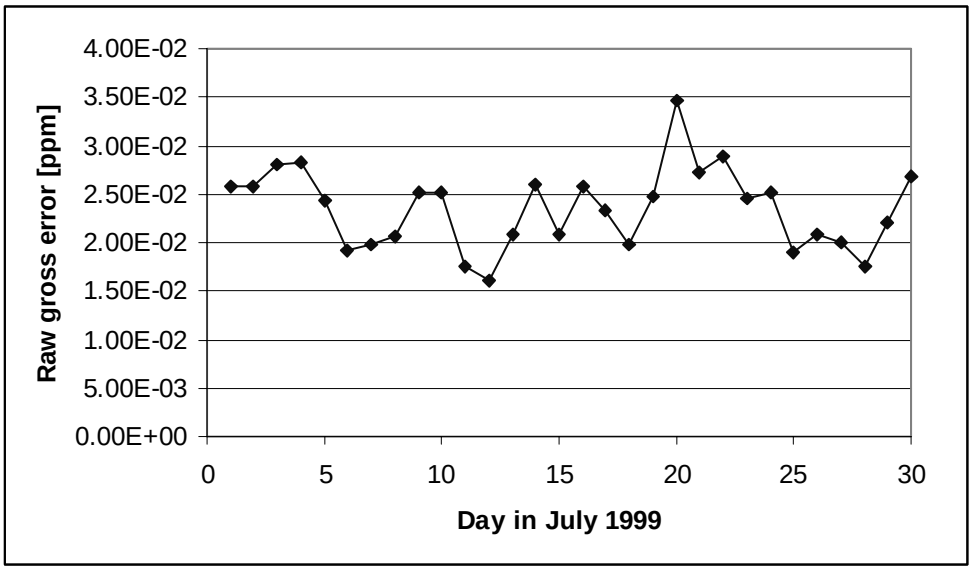

Figure 5: Raw gross error as a function of simulation day. Raw gross error:

$\frac{1}{N}\sum_{i=1}^{N}\left|X_{p,i}(t) - X_{o,i}(t)\right|$, where X_p is the modeled and X_o is the measured mixing ratios.

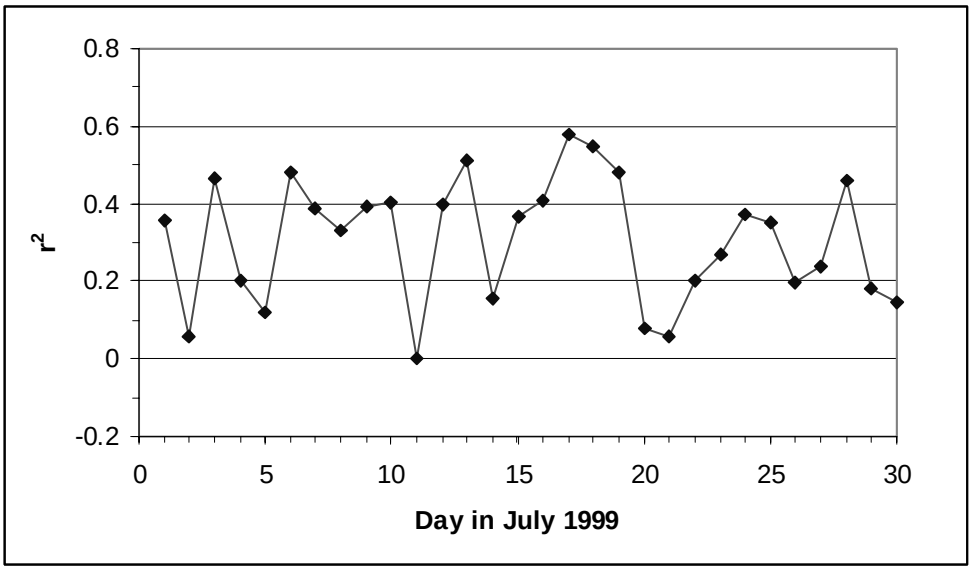

Figure 6: Coefficient of determination between observed and modeled ozone as a function of simulation day.

Chapter 4

THE SENSITIVITY OF SULFUR WET DEPOSITION TO ATMOSPHERIC OXIDANTS

The formation of ozone and other atmospheric oxidants mediates the transformation of pollutants such as sulfur dioxide (SO_2) into aerosol sulfate (SO_4^{2-}) and is chemically linked to the emissions of nitrogen oxides (NO_x) and volatile organic compounds (VOC). In this chapter we intend to gain understanding of the linkages between sulfate formation and oxidant chemistry and transport through a case study in which large amounts of sulfate were measured and modeled.

Methods

Measurements

Some atmospheric and all precipitation chemistry sampling was performed at the Penn State research station at Scotia (40^o 47' N and 77^o 59' W). A particularly valuable attribute of this site is its rural setting in central Pennsylvania, as all significant point sources of sulfurous pollution are in excess of 40 km from the sampling site. Lamb and Comrie (1993) have given a detailed description of the site. Precipitation there has been collected for chemical analysis since 1976, originally as part of the Multistate Atmospheric Power Production Pollution Study (MAP3S; MacCracken, 1978), but later

under the "daily" sampling protocols of the Atmospheric Integrated Research Monitoring Network (AIRMoN; Rothert *et al*., 1997; http://www.arl.noaa.Gov/ research/programs/ airmon.html), a component of the National Atmospheric Deposition Program (NADP; http://nadp.sws.uiuc.edu/). Precipitation chemistry data for this study day were obtained from the NADP Program Office in Champaign, IL (http://nadp.sws.uiuc.edu/airmon/). The Penn State site has also been used to monitor SO_2 continuously since 1988 and particulate sulfate since 1991.

The atmospheric measurements were made using conventional instrumentation and methods. Sulfur dioxide mixing ratios were measured with a fluorescence detector (Monitor Labs Model 8850) having a lower detection limit of 1 ppb. The SO_2 analyzer is calibrated once a month using a sulfur dioxide permeation tube (GC Industries) as a standard. The concentration of particulate sulfate was measured with a flame-photometric detection system (Meloy 185-2) that responds to all sulfur compounds (Tanner *et al.*, 1980). The system is made selective for particulate sulfate by drawing sample air first through a denuder tube coated with PbO_2 to remove gaseous sulfur compounds. The SO_4^{2-} analyzer is calibrated once a month using an SF_6 gas delivery system as the standard.

Ozone (O_3) data were collected at the Pennsylvania State University Agricultural Research Center at Rock Springs (40^o 43' N and 77^o 56' W). This site is located approximately 8 km south of Scotia and resides in the same open valley. Due to the regional-scale influence that ozone has over rural areas, the measurements at Rock Springs should represent the O_3 levels at Scotia adequately (Shreffler and Barnes, 1996).

Ozone measurements were performed using an ultraviolet photometric analyzer (Thermo Electron Instruments Model 49), the lower detection limit of which is 2 ppb.

Model description

In order to assess the principal processes by which ambient sulfate is formed we used a trajectory-type air quality simulation model. The U.S. Environmental Protection Agency's (EPA) Ozone Isopleth Plotting Research (OZIPR) program (Gery and Crouse, 1991) was employed toward that end to simulate a well-mixed column of air extending from the ground to the top of the boundary layer. Whereas the column cannot expand horizontally, it does vary in vertical extent in response to changes in the depth of the mixed layer. This idealized column moves along a specified wind trajectory, one that is calculated from the Hybrid Single-Particle Lagrangian Integrated Trajectory (HY-SPLIT_4) model of Draxler and Hess (1998). Input wind fields were obtained from a standard meteorological forecast model, the Nested Grid Model (NGM; Phillips, 1975; Hoke *et al.*, 1989) of the National Center for Environmental Prediction.

The chemistry employed in the OZIPR model was based on various sources of information. Primary emissions of SO_2, NO_x, RH, carbon monoxide (CO), and isoprene were calculated at the county level on an annual basis from EPA's National Emission Trends Viewer (1998) and used to update the concentrations of precursors in the model column as it moves along the prescribed trajectory. The Regional Acid Deposition Model (RADM2) chemical mechanism (Stockwell *et al.*, 1990) was used to describe the gas-phase chemical processes that occurred within the modeled air, whereas the aqueous-phase SO_2-oxidation reactions of Stockwell (1994a) were used for in-cloud

transformations. When appropriate, in order to simulate non-precipitating clouds encountered by the idealized column of air along a trajectory, the aqueous-phase was fixed at a liquid water volume fraction $\nu_L = 1x10^{-6}$, a value typical for many clouds (Finlayson-Pitts and Pitts, 1986, pp. 665) and a pH of 4. Aqueous-phase rate constants and concentrations of chemical species were converted into their equivalent gas-phase values using the specified value of ν_L as a conversion factor (Jacob, 1986). All species that experience partitioning between the liquid and gas phase were assumed to obey Henry's law (Seinfeld and Pandis, 1998, p. 340). We also assumed that the sulfate formed in the aqueous phase was transferred as ambient sulfate to the air (due to the evaporation of the droplets) whenever rain was not present.

This modeling approach, though simple, captures the main features of oxidant formation, as well as SO_2 oxidation in clear air and in non-precipitating clouds. This approach, while limiting in some respects, is adequate for evaluating the response of the reactive air parcel to a variable set of input conditions. Similar models have already been successfully employed to estimate H_2O_2 levels within the planetary boundary layer (Tremmel *et al*., 1993; Weinstein-Lloyd *et al*., 1998; Wangteng *et al*., 1991). However, some physical processes that could influence SO_4^{2-} formation are not fully considered by OZIPR. For instance, interactions between the planetary boundary layer and the free troposphere and the effects of deep convective clouds on the spatial redistribution of SO_2 and H_2O_2 are not taken into account. Nevertheless, mixing free tropospheric air with boundary layer air would clearly increase the fraction of SO_2 that can be oxidized, but not

to the point of reversing the behavior, such that previously oxidant-limited cases become non-oxidant-limited cases (Kleinman and Daum, 1991).

Case study

Episode description

On 17 June 1996 a heavy rain event took place in the vicinity of State College, Pennsylvania. A maximum observed rain amount of 130 mm occurred in the southwestern part of the town, about 8 km east of the Scotia sampling site. The rain event began at 16:30 EST (20:30 UTC) and lasted approximately 2 hours. Table 1 shows the precipitation amount and the concentrations of the principal ions sampled under the NADP/AIRMoN protocol at Scotia for that date. A peculiar characteristic of this episode was the low pH and the elevated concentration of SO_4^{2-} measured in the rain. The lower atmosphere had been extremely hazy throughout the day, and high levels of O_3 and ambient SO_4^{2-} were recorded prior to this rain event, as detailed below.

From the available meteorological information, an east-west stationary front was located over southern Pennsylvania from 17 June to 18 June 1996, as shown in Figure *7*. This synoptic situation forced air masses to move slowly and be confined to the western portions of Pennsylvania (dashed curve in Figure *7*). This stagnant airflow presumably favored the accumulation of SO_2 and its oxidation to SO_4^{2-}. Figure 8 (a) and (b) show the measured SO_2, ambient SO_4^{2-}, and O_3 mixing ratios for the day of the event. The shape of the SO_2 mixing ratio curve can be partially explained in terms of the variation of the mixed-layer depth with the time of day. At night, when the boundary layer collapses and a nocturnal inversion forms just above the surface, SO_2 in the lowest layer typically

Table 1: Data and the concentrations of selected ions pertaining to the rain event of 17 June 1996 in State College, PA.

Date	Precipitation [mm]	pH	NO_3^- [μM]	SO_4^{2-} [μM]	NH_4^+ [μM]
June 17 1996	66	3.7	70 (4.6)[a]	105 (6.9)[a]	58 (3.8)[a]

[a] The values in parenthesis correspond to the deposition in mmol/m^2.

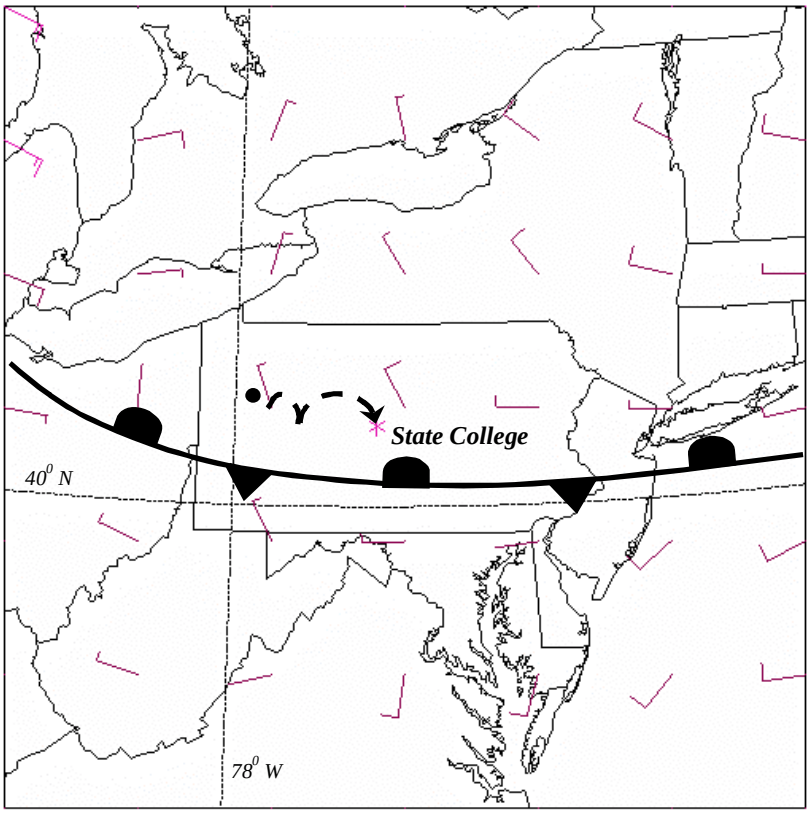

Figure 7: 24-hour back-trajectory calculation ending 20:00 UTC 17 June 1996 (dashed curve). The stationary front, as well as wind flags at approximately 1000 m (National Meteorological Center's NGM; Phillips (1975); Hoke *et al.* (1989)), are also shown.

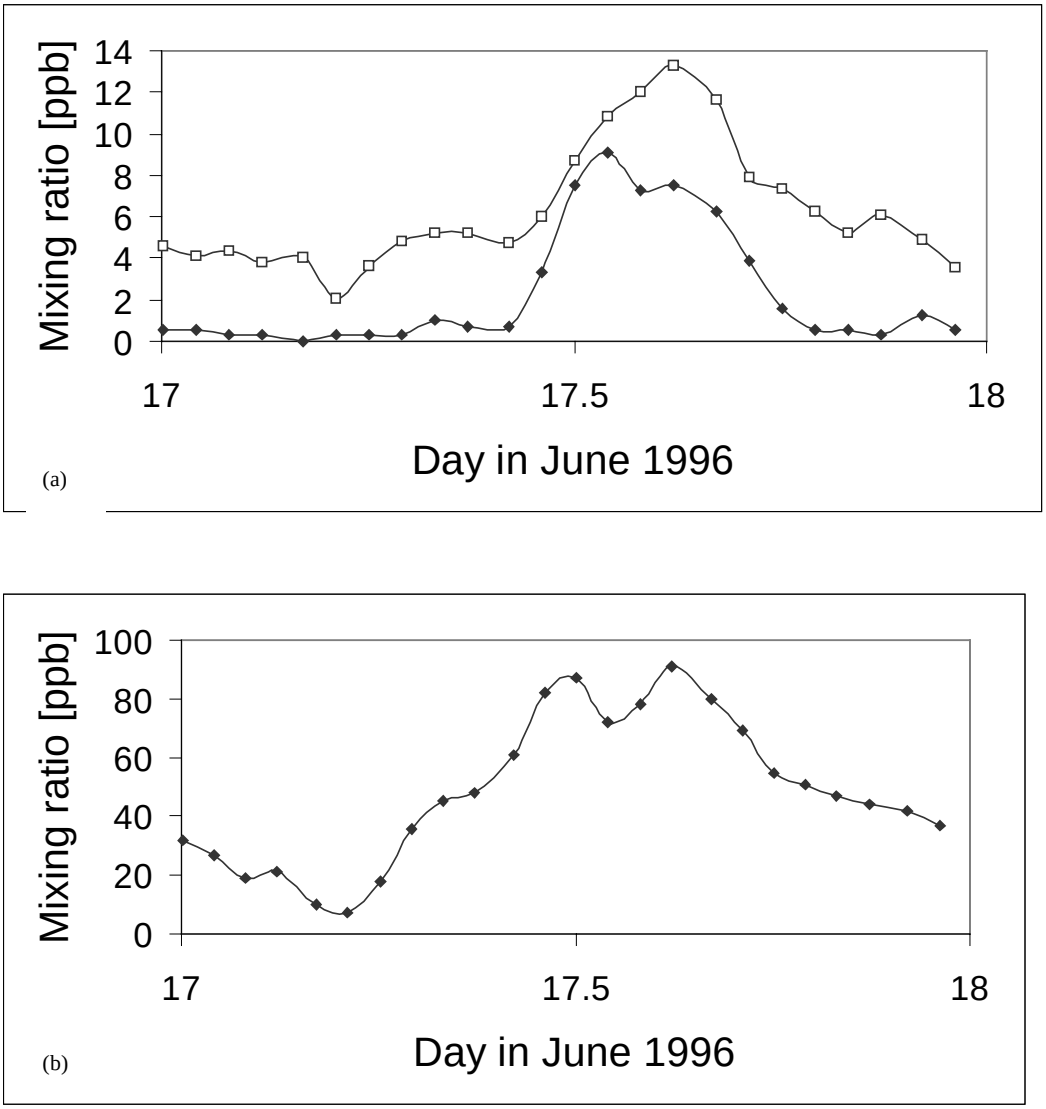

Figure 8: Observed mixing ratios for 17 June 1996. (a) SO_2 (black diamonds) and ambient SO_4^{2-} (open squares) at the Scotia site. (b) O_3 at Rock Springs.

becomes depleted by dry deposition, thus explaining the low nocturnal mixing ratios measured near the surface. However, in the "residual" layer above, which does not have direct contact with the ground, this gas can persist throughout the night (Trainer *et al.*, 1991). The reconnection of the residual layer of the previous night with the top of the growing mixed layer in the morning temporarily fumigates the surface with a finite amount of SO_2. Further growth of the convective boundary layer rapidly dilutes the sulfur dioxide, resulting in a maximum toward midday. The subsequent decline results from a combination of dry deposition at the surface and increased photochemical conversion during the day. On the other hand, the O_3 and ambient SO_4^{2-} curves show signs that are indicative of photochemical activity in addition to the effects of the physical boundary layer processes (e.g., Trainer *et al.*, 1991). The minimum at night reflects the formation of an inversion layer, as in the case for SO_2. The first daytime peak in the O_3 curve might be the result of fumigation from the residual layer.

Simulation of the episode

The main chemical and physical factors that influence the formation of ambient SO_4^{2-} were investigated with the OZIPR model for the conditions of the episode. All simulations began at 08:00 EST (12:00 UTC) and were made to follow the trajectory calculated by HY-SPLIT_4 (Figure 7). The depth of the mixed layer was set to 600 m at the beginning of the calculation and reached its maximum value of 1800 m at 15:00 EST (19:00 UTC). The initial conditions used for the simulations are shown in Table 2. For the first part of the study, only gas-phase reactions with sulfur dioxide were included in the simulation. In this case, the maximum ambient SO_4^{2-} mixing ratio was

Table 2: Initial conditions used to simulate the event.

SO_2 [ppb]	Ambient SO_4^{2-} [ppb]	NO_x [ppb]	RH [ppbC]	O_3 [ppb]
5 (15)[b]	4	10[a]	50	50 (40)[b]

[a] estimated from Trainer *et al*. (1991).
[b] mixing ratios aloft.

Table 3: Comparison between peak values of measured and modeled variables [ppb].

	SO_2	Ambient SO_4^{2-}	O_3
Measurement	6.2	13.3	80
Model without aqueous-phase chemistry	10.7	6.6	79
Model with aqueous-phase chemistry	6.8	10.4	79

underestimated and the SO_2 mixing ratio was overestimated by the model when compared with the measured values at the beginning of the rain (Table 3). Gas-phase reactions alone are not able to explain the measured abundance of ambient SO_4^{2-} during this event.

When aqueous-phase SO_2 oxidation reactions were included in the chemical simulation, the SO_2 and ambient SO_4^{2-} mixing ratios obtained by the model came into closer agreement with the measurements (Table 3). The slight discrepancy between the total sulfur measured and that calculated by the model (12%) is probably due to the lack of an accurate set of initial conditions for the simulation. The principal aqueous-phase reaction that produced SO_4^{2-} was the oxidation of SO_2 by H_2O_2. This reaction is very fast, and indeed both field measurements (Van Valin *et al*., 1991; Daum *et al*., 1984) and theoretical studies (Pandis and Seinfeld, 1989) have suggested that H_2O_2 and SO_2 rarely coexist in clouds. The species with the lowest concentration before cloud formation is the limiting reactant and is rapidly depleted inside the cloud. This result is in accord with previous studies that have established the need to include the in-cloud oxidation of SO_2 in order to account for observed concentrations of ambient SO_4^{2-} (Dennis *et al*., 1993).

In order to relate the ambient SO_4^{2-} mixing ratios to the aqueous-phase concentrations of sulfate observed in rain, we use the concept of a "scavenging factor" *F* (Pruppacher and Klett, 1997, p. 785). This dimensionless parameter is defined as the ratio of the atmospheric concentration of scavenged SO_4^{2-} in rainwater to the concentration of aerosol sulfate in the air. Thus,

$$F_{SO_4^{2-}} = \frac{[SO_4^{2-}]_{rain} \times v_L}{[SO_4^{2-}]_{air}} \quad , \qquad (4\text{-}1)$$

where $v_L = \omega_L / \rho_{H_2O}$ is the liquid water fraction, ω_L is the liquid water content [g m^{-3}] and ρ_{H_2O} is the density of water. To estimate the value of $F_{SO_4^{2-}}$ for this particular event we used Equation (1) with ω_L = 3 g m^{-3} (estimated from Wang and Crutzen, 1995), $[SO_4^{2-}]_{air}$ = 5.6x10^{-7} mol m^{-3} of air (equivalent to 13 ppb), and $[SO_4^{2-}]_{rain}$ = 1.05x10^{-4} mol L^{-1} of water. The value of the calculated scavenging factor, $F_{SO_4^{2-}}$ = 0.6, is within the range of those found in the literature. For instance, Hegg *et al.* (1984) and Hegg and Hobbs (1986, 1988) have shown that 0.5 < $F_{SO_4^{2-}}$ < 0.8. Also, Dutkiewicz and Husain (1998) found a mean $F_{SO_4^{2-}}$ of 0.6 for $[SO_4^{2-}]_{air}$ > 5x10^{-8} mol m^{-3} of air. Regardless of the specific value of $F_{SO_4^{2-}}$, according to Equation (1), the sulfate concentration in the rain will be proportional to the ambient SO_4^{2-}. This behavior allows us to make the assumption that any conclusion about the variation of the SO_4^{2-} concentration in the air is going to be applicable to the SO_4^{2-} in the rain, hence to the wet deposition of sulfate.

These results indicate that the aqueous-phase oxidation of SO_2 by hydrogen peroxide in upwind, non-precipitating clouds is likely to be the dominant mechanism for the formation of sulfate in this event. Also, this modeling exercise shows that hydrogen peroxide is the species in lesser abundance (< 4 ppb when compared with SO_2 before any influence of the aqueous-phase chemistry), so the system is likely to have been oxidant limited. Indeed, prior measurement studies (Dutkiewicz *et al.*, 1995; Kleinman and Daum, 1991) suggest that oxidant-limited conditions are often found in the eastern U.S. Therefore, the levels of H_2O_2 in the air have a strong influence over the amounts of SO_4^{2-} to be formed.

In order to explore the response of ambient SO_4^{2-} to changes in H_2O_2 precursors, we ran the OZIPR model for a series of NO_x and VOC emission rates, keeping the rest of the variables the same as used to simulate the event of 17 June. The results are shown in Figure 9 as an isopleth plot of ambient sulfate. For moderate and high NO_x emissions, the calculated mixing ratio of ambient SO_4^{2-} actually increases as the abundance of NO_x decreases. Only for low-NO_x conditions do the mixing ratios of SO_4^{2-} decrease as the levels of NO_x decrease. This behavior can be understood in terms of the chemical interactions that give rise to the formation of ambient sulfate. Hence, in the next chapter we investigate the chemical relationship between concentrations of the SO_2 oxidants and their precursors.

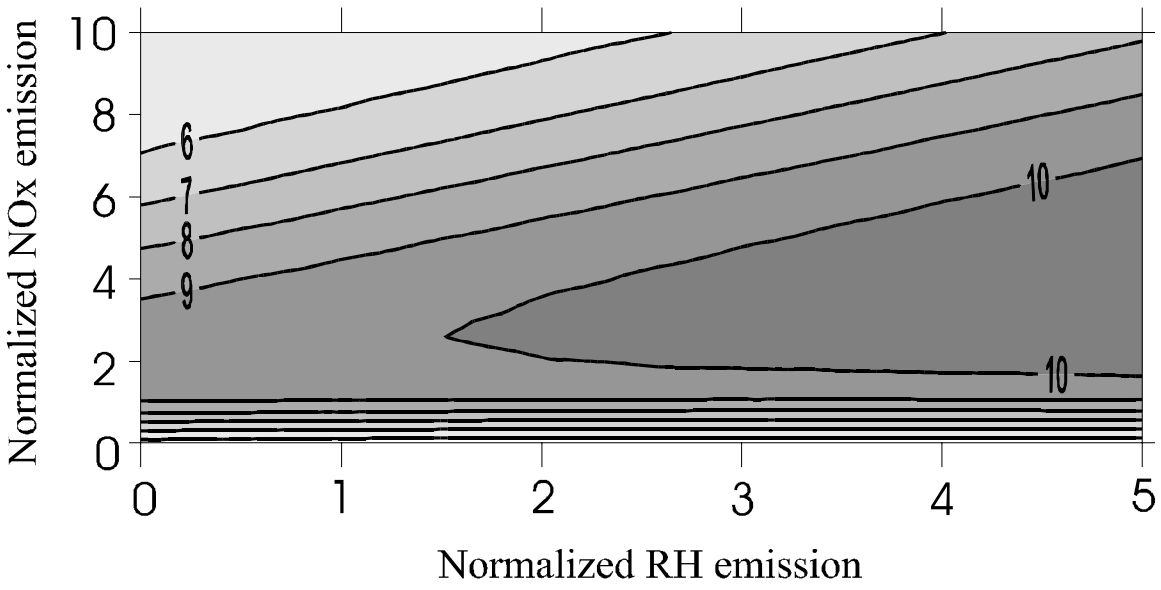

Figure 9: Isopleth plot showing calculated maximum ambient SO_4^{2-} mixing ratios [ppb] obtained from various initial VOC and NO_x mixtures.

Chapter 5

CHEMICAL INDICATORS OF SULFATE SENSITIVITY TO NITROGEN OXIDES AND VOLATILE ORGANIC COMPOUNDS

Sensitivity of SO_4^{2-} to changes in NO_x and VOC abundance

Review of the relevant chemistry

For the purposes of this study only a brief description of the relevant chemical reactions that account for sulfate formation in industrialized areas is given. More extensive reviews can be found elsewhere (e.g., Sakugawa *et. al.*, 1990; Kleinman, 1991, Stockwell, 1994a). The gas-phase (clear-air) formation of sulfate occurs through a reaction between SO_2 and the hydroxyl radical (OH; Stockwell and Calvert, (1983)), namely

$$SO_2 + OH \rightarrow SO_4^{2-} + HO_2. \qquad \text{(RG)}$$

The OH radical is generated from ambient ozone by the following reactions:

$$O_3 + h\nu \rightarrow O(^1D) + O_2 \qquad \text{(R1)}$$

$$O(^1D) + H_2O \rightarrow 2\ OH\ , \qquad \text{(R2)}$$

and it is removed primarily by

$$OH + NO_2 \xrightarrow{M} HNO_3\ . \qquad \text{(R3)}$$

Once nitric acid (HNO_3) is formed it can reside in the gas phase or may be transferred to the particulate phase in its ionic form (nitrate, NO_3^-).

By contrast, the aqueous-phase (in-cloud) production of sulfate, while more complicated than the clear-air mechanism, can be represented by the following overall reaction involving hydrogen peroxide (H_2O_2; Stockwell, (1994a)):

$$SO_2 + H_2O_2 \xrightarrow{\text{cloud}} SO_4^{2-}. \qquad \text{(RA)}$$

Field measurements (Van Valin *et al*., 1991; Daum *et al*., 1984), as well as theoretical studies (Pandis and Seinfeld, 1989), have suggested that reaction RA is very fast, so H_2O_2 and SO_2 rarely coexist in clouds. Furthermore, H_2O_2 is formed in the atmosphere from the recombination of hydroperoxyl radicals (HO_2; Kleinman, (1991)):

$$HO_2 + HO_2 \rightarrow H_2O_2 + O_2 \ . \qquad \text{(R4)}$$

Reaction R4 exhibits complicated dependencies on pressure, water vapor concentration and temperature (Stockwell, 1994b). The hydroperoxyl radical is produced and destroyed in a series of chain reactions involving VOC (particularly hydrocarbons), carbon monoxide (CO) and NO_x (Seinfeld and Pandis, 1998, p. 264):

$$OH + VOC \xrightarrow{O_2} RO_2 + H_2O \qquad \text{(R5)}$$

$$OH + CO \xrightarrow{O_2} HO_2 + CO_2 \qquad \text{(R6)}$$

$$RO_2 + NO \rightarrow HO_2 + NO_2 + R'CHO \qquad \text{(R7)}$$

$$HO_2 + NO \rightarrow OH + NO_2 \qquad \text{(R8)}$$

$$RO_2 + HO_2 \rightarrow ROOH + O_2 \ . \qquad \text{(R9)}$$

Moreover, the photolysis of formaldehyde and higher aldehydes ($R'CHO$) constitute additional sources of the HO_2 radical:

$$H_2CO + h\nu \xrightarrow{O_2} HO_2 + HCO \quad \text{(R10)}$$

$$HCO + O_2 \rightarrow HO_2 + CO \quad \text{(R11)}$$

$$R'CHO + h\nu \xrightarrow{O_2} HO_2 + R'CO \quad \text{(R12)}$$

Careful analysis of the chemistry, as given above and depicted schematically in Fig. 10, reveals some of the complexity that emerges when parts of the system change. For instance, the photolysis of aldehydes (reactions R10 through R12; right-hand side of Fig. 10) and the oxidation of hydrocarbons (reactions R5 and R7) lead directly to the formation of HO_2 and indirectly to H_2O_2 generation (*via* reaction R4). Thus, the ambient concentration of particulate sulfate formed *via* aqueous-phase oxidation is likely to decrease in response to any decrease in hydrocarbon levels. However, for any given abundance of VOC, the sulfate formed in the liquid phase may show a contrasting behavior when the levels of NO_x change. That is, under moderate-to-high NO_x levels a decrease in NO_x levels would lead to an *increase* in SO_4^{2-} formation due to a shift away from the formation of HNO_3 and toward an increase in the peroxides production rates (reactions R9 and R4, in contrast to R3, the main sink of OH; left-hand side of Fig. 10). Not until the NO_x levels become very low would we expect in-cloud sulfate formation to decrease in direct response to decreases in NO_x emissions (Stein and Lamb, 2000). These viewpoints are valid only under the assumption that oxidant-limited conditions prevail, i.e., that the SO_2 concentration is higher than that of H_2O_2 (Kleinman and Daum, 1991). Nevertheless, we can avoid this restriction and regard these ideas as generally valid by using the concept of “potential” sulfate. Potential sulfate, defined as the sum of ambient sulfate and H_2O_2 (Stockwell, 1994a), can be interpreted as the maximum

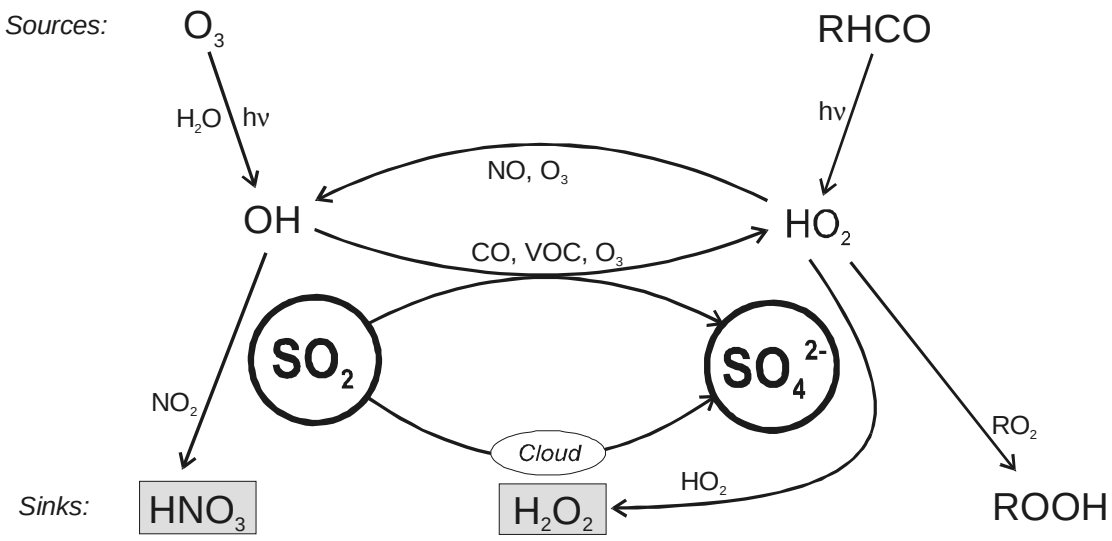

Figure 10: Chemical cycle of OH and HO_2 coupled with the oxidation of SO_2.

concentration of SO_4^{2-} that could be produced in the gas and aqueous phases. Therefore, in this work we will consider ambient sulfate to be equivalent to potential sulfate.

The gas-phase formation of ambient sulfate, on the other hand, may present a different response to changes in VOC emissions when compared to the in-cloud oxidation pathway. For given low-to-moderate NO_x levels, clear-air SO_4^{2-} formation is likely to increase in response to decreases in VOC emissions. This behavior reflects the competition between VOC and NO_2 for the OH radical (left-half of Fig. 10), the main clear-air SO_2 oxidant (Calvert *et al.*, 1978; Eggleton and Cox, 1978). For high NO_x levels, the SO_4^{2-} formed through gas-phase oxidation is likely to decrease as VOC emissions are lowered. Finally, for any given level of VOC, the clear-air sulfate production shows a similar response to that of the in-cloud oxidation for changes in NO_x levels.

We can thus identify two photochemical regimes, each of which exhibits a different response of potential SO_4^{2-} production to changes in NO_x and VOC emissions, depending on the main sink of odd-hydrogen, defined as the sum of OH, HO_2, and organic peroxyl (RO_2) radicals (Sillman, 1995). When the formation of HNO_3 dominates the loss of odd-hydrogen, a decrease in NO_x frees up the OH that can react with SO_2, CO, and VOC, which thus increases the abundance of HO_2 that in turn favors the formation of H_2O_2. Consequently, the interaction of these reactions tends to increase the formation of SO_4^{2-} via both the clear-air and aqueous-phase pathways. A decrease in VOC levels would reduce OH by making it available to form more HNO_3. As a consequence, the

H_2O_2 production would also be reduced, thus decreasing the formation of SO_4^{2-}. Under this photochemical regime, called "VOC-sensitive", potential SO_4^{2-} decreases with decreasing VOC and *increases* with decreasing NO_x.

By contrast, when the formation of HNO_3 can be regarded as a small odd-hydrogen sink, a decrease in NO_x concentrations would slow down the conversion of HO_2 to OH (middle part of Fig.10), thereby decreasing the overall SO_4^{2-} formation. When the VOC levels are lowered, a small amount of OH would be available to react with SO_2, slightly increasing the gas-phase production of SO_4^{2-}. Lowering the VOC concentrations would not significantly affect the formation of H_2O_2, however, due to the fact that the system is saturated with hydrocarbons. Therefore, the aqueous-phase SO_2 oxidation would remain unaltered. This scenario constitutes the "NO_x-sensitive" photochemical regime, in which aerosol SO_4^{2-} concentrations would decrease with decreasing NO_x and would be largely independent of VOC. The highly nonlinear and coupled nature of the sulfate production process is responsible for this somewhat counter-intuitive behavior.

Milford *et al* (1994) and Sillman (1995) have developed a methodology to assess the sensitivity of ozone to changes in NO_x and VOC. They found that model predictions for O_3-NO_x sensitivity were associated with the concentrations of a number of key chemical species that differed from those linked to O_3-VOC sensitivity. Milford *et al*. (1994) showed that ozone simulated under an NO_x-sensitive regime was linked to afternoon values of total reactive nitrogen (NO_y) below a certain threshold concentration, while VOC-sensitive ozone was connected to higher NO_y levels. Sillman (1995) extended that work to include species ratios, such as O_3/NO_y and H_2O_2/HNO_3. Following these

ideas, we propose the use of a combination of model-simulated afternoon concentrations of HNO_3, H_2O_2, and ambient SO_4^{2-} as "indicator species" of the ambient SO_4^{2-}-VOC-NO_x sensitivity.

Theoretical Relationships

The steady-state balance of odd-hydrogen (HO_x) constitutes the basis for understanding the response of the $[H_2O_2]$ + $[SO_4^{2-}]$ concentrations to changes in the VOC and NO_x emissions. Sillman *et al.* (1990) showed that the composite set of sources and sinks of HO_x can be interrelated via the following continuity relationship:

$$S_{HOx} = 2k_4[HO_2]^2 + 2k_9[HO_2][RO_2] + k_3[OH][NO_2] + P_{PAN} \quad , \quad (5\text{-}1)$$

where S_{HOx} represents the source of HO_x from the photolysis of ozone (reactions R1 and R2) and aldehydes (e.g., reaction R10). The first and second terms on the right hand side of Equation (5-1) represent a sink of HO_2 and RO_2 through the formation of H_2O_2 and organic peroxides, respectively. The third term represents the production of HNO_3 (P_{HNO3}), the main sink for OH. Finally, P_{PAN} represents the sink from peroxyacetilnitrate (PAN) formation.

Equation (5-1) can be expanded under some conditions. When S_{HOx} and P_{PAN} can be expressed as proportional functions of the production rate of O_3 (P_{O3}) (Sillman, 1995), defined as

$$P_{O3} = k_5 [VOC] [OH] / X \quad , \quad (5\text{-}2)$$

where $X = k_5 [VOC] / (k_6 [CO] + k_5 [VOC])$, and also when the concentrations of $[HO_2]$ and [OH] are in steady-state, Equation (5-1) can be rewritten as

$$\frac{f_{HOx}k_5[\mathrm{VOC}][\mathrm{OH}]}{X} = 2\frac{k'k_5^2}{X^2}\left\{\frac{[\mathrm{VOC}]}{[\mathrm{NO_x}]}\right\}^2[\mathrm{OH}]^2 + k_3w_2[\mathrm{OH}][\mathrm{NO_x}] + \frac{f_{PAN}k_5[\mathrm{VOC}][\mathrm{OH}]}{X} \qquad ,(5\text{-}1')$$

where $f_{HOx} = S_{HOx}/P_{O3}$,

$f_{PAN} = P_{PAN}/P_{O3}$,

$k' = k_4/(k_8^2w_1^2) + k_9X/(k_7k_8w_1^2)$,

$w_1 = [\mathrm{NO}]/[\mathrm{NO_x}]$, and

$w_2 = [\mathrm{NO_2}]/[\mathrm{NO_x}]$.

On the other hand, the gas-phase sulfate production rate is given by

$$P_{SO4G} = k_G[\mathrm{SO_2}][\mathrm{OH}] \ . \qquad (5\text{-}3)$$

In a similar way we define the production rate of H_2O_2 formation as (Stein and Lamb, 2000)

$$P_{H2O2} = k_4[\mathrm{HO_2}]^2 \qquad , \qquad (5\text{-}4)$$

which can be related to the in-cloud sulfate formation by realizing that all the H_2O_2 formed could potentially produce SO_4^{2-}. Thus, making use of the concept of "potential" sulfate (Stockwell, 1994a), we have

$$P_{SO4} = P_{H2O2} + P_{SO4G} \ , \qquad (5\text{-}5)$$

where P_{SO4} represents the overall production of "potential" sulfate. Substituting Equation (5-3) into (5-1') gives

$$P_{SO4G} = \left[\left(f_{HOx} - f_{PAN}\right)\frac{k_5[\mathrm{VOC}]}{X} - k_3w_2[\mathrm{NO_x}]\right]\frac{X^2[\mathrm{NO_x}]^2k_G[\mathrm{SO_2}]}{2k'k_5^2[\mathrm{VOC}]^2} \qquad . \qquad (5\text{-}6)$$

Analogously, by substituting Equation (5-4) into (5-1') and assuming that the steady state balance between [OH] and [HO_2] holds, we obtain

$$P_{\mathrm{H2O2}} = \left\{ \left[\left(f_{HOx} - f_{PAN} \right) \frac{k_8 w_1 [\mathrm{NO_x}]}{k_4^{1/2}} - \frac{X k_3 w_1 w_2 k_8 [\mathrm{NO_x}]^2}{k_4^{1/2} k_5 [\mathrm{VOC}]} \right] \frac{k_4}{2k' k_8^2 w_1^2} \right\}^2 \quad . \qquad (5\text{-}7)$$

The threshold value for the transition between the VOC- and NO_x-sensitive regimes can be calculated by equating the partial derivatives for P_{SO4} with respect to a fractional change in VOC and NO_x, namely

$$[\mathrm{NOx}] \frac{\partial P_{\mathrm{SO4}}}{\partial [\mathrm{NOx}]} = [\mathrm{VOC}] \frac{\partial P_{\mathrm{SO4}}}{\partial [\mathrm{VOC}]} \quad . \qquad (5\text{-}8)$$

Substituting Equations (5-5), (5-6), and (5-7) into (5-8), we obtain

$$\left. \frac{P_{\mathrm{H2O2}}}{P_{\mathrm{HNO3}}} \right|_{Threshold} = k_* \left[\frac{2 - x_{SO4G}}{2 + x_{SO4G}} \right] \quad , \qquad (5\text{-}9)$$

where $k_* = k_4/(k' k_8^2 w_1^2)$, and $x_{SO4G} = P_{\mathrm{SO4G}}/(P_{\mathrm{H2O2}}+P_{\mathrm{SO4G}})$. However, this expression cannot be used in its present form because P_{H2O2} could include a portion of sulfate that is formed by in-cloud oxidation of SO_2. Hence, we would need additional information about the fraction of sulfate formed in the gas phase compared to the in-cloud production to make use of the $P_{\mathrm{H2O2}}/P_{\mathrm{HNO3}}$ ratio as an indicator. We can circumvent this inconvenience by adding the $P_{\mathrm{SO4G}}/P_{\mathrm{HNO3}}$ ratio to both sides of Equation (5-9) to obtain

$$\left.\frac{P_{\mathrm{SO4}}}{P_{\mathrm{HNO3}}}\right|_{Threshold} = k_{*}\left[\frac{2 - x_{SO4G}}{(1 - x_{SO4G})(2 + x_{SO4G})}\right] \quad . \qquad (5\text{-}10)$$

This is the expression for the transition point between NO_x- and VOC- sensitivity for "potential" sulfate. The right hand side of Equation (5-10) is bounded by values between 1 and 2 for x_{SO4G} lower than 80%, a condition that for atmospheric conditions generally holds. Therefore, for all practical purposes, the threshold value for P_{SO4}/P_{HNO3} is approximately constant. This finding constitutes the theoretical rationale for using the ratio of $\{[H_2O_2]+[SO_4^{2-}]\}/\{[HNO_3]+[NO_3^-]\}$ as the indicator for "potential" SO_4^{2-}-VOC-NO_x sensitivity.

The link between the indicator and the NO_x-VOC chemistry can be further understood in terms of the dominant sinks and sources for odd-hydrogen. The NO_x-sensitive regime favors the formation of "potential" sulfate over the production of HNO_3. Under this condition the production of H_2O_2 constitutes the main loss of HO_x through reaction (R4). Also, under NO_x-sensitive conditions the gas-phase SO_2 oxidation (Reaction RG) is favored. On the other hand, the VOC-sensitive regime is characterized by a high production rate of HNO_3 that overwhelms the formation of "potential" sulfate.

Alternatively, for situations in which the in-cloud formation of sulfate can be regarded as negligible when compared with the gas-phase path (as during cloud-free days), a particular solution of the "potential" sulfate sensitivity threshold can be found. Under this assumption the production of total sulfate is simply equal to the gas-phase production of sulfate. Therefore, we can recalculate the transition indicator ratio by

equating the partial derivatives of P_{SO4G} with respect to the fractional change in NO_x and VOC, namely

$$[\mathrm{NOx}]\frac{\partial P_{\mathrm{SO4G}}}{\partial[\mathrm{NOx}]} = [\mathrm{VOC}]\frac{\partial P_{\mathrm{SO4G}}}{\partial[\mathrm{VOC}]} \quad . \qquad (5\text{-}11)$$

Then substituting Equation (5-6) into (5-11) we obtain

$$\left.\frac{P_{\mathrm{H2O2}}}{P_{\mathrm{HNO3}}}\right|_{Threshold} = \frac{1}{3}k_{*} \quad , \qquad (5\text{-}12)$$

and the $[H_2O_2]/[HNO_3]$ ratio could be used as an indicator of the sulfate VOC-NO_x sensitivity for particular atmospheric conditions that only favor the formation of sulfate via gas-phase SO_2 oxidation.

Simulation

In order to investigate the response of "potential" sulfate to changes in the NO_x and VOC source strengths we make use of U.S. Environmental Protection Agency (EPA)'s MODELS-3 (Dennis *et al*., 1996) Personal Computer (PC) version. This system constitutes a state-of-the-art tool for regional-scale simulations of photochemical smog, visibility and fine particulates. MODELS-3 is a versatile software system that includes a Community Multiscale Air Quality (CMAQ) model (EPA, 1999b). CMAQ is a three-dimensional Eulerian chemical transport model that accounts for horizontal and vertical advection, eddy diffusion, gas-phase chemical transformations, emissions, cloud mixing,

aqueous-phase chemical reactions, and aerosol processes. The meteorological data used by this simulation are obtained as output fields from the Mesoscale Model Version 5 (MM5) (Grell *et al*., 1994, Seaman and Michelson, 2000). Emissions are calculated by the MODELS-3 Emissions Processing and Projection System (MEPPS) (EPA, 1999b). A detailed description of the equations and algorithms of each component of MODELS-3 are given by EPA (1999b).

The simulation results presented here are based on an air pollution event that took place over the eastern United States during July 12-14, 1995. This episode featured concentrations exceeding the 1-h NAAQS for ozone with a maximum of 175 parts per billion (ppb) measured at a Connecticut site on July 14 (Sistla *et al.*, 2001). In order to allow the model to build up the chemical species concentrations minimizing the influence of initial conditions, the first two simulation days are considered as the initialization period. Therefore, only the results for July 14 are discussed in this study. The model domain covered an area of 2268 x 2808 km^2 from the Great Lakes and northern New England to the Gulf of Mexico with a 36-km resolution. The simulation utilized 15 non-hydrostatic sigma-pressure vertical layers. Initial concentrations and boundary conditions were set to near-rural conditions (Chang *et al.*, 1990). The RADM2 chemical mechanism (Stockwell *et al*., 1990) was used to simulate the gas-phase chemical reactions. The aerosol processes were calculated based on the Regional Particulate Model (RPM) (Binkowski and Shankar, 1995). Area and point emissions were estimated using MEPPS based on the 1995 National Emissions Trends (EPA, 1999b). Emissions data from motor

vehicles and vegetation were simulated using the Mobile5a (EPA, 1996b) and BEIS-2 (Pierce *et al*., 1998) models, respectively.

The meteorological data used for the present case study are described in detail in Seaman and Michelson (2000), so only a brief summary is given here. This event featured light winds, restricted vertical mixing and high temperatures associated with the Bermuda high. Besides, mesoscale structures associated with an Appalachian lee trough played a key role in determining the geographical distribution of photochemical smog. Low mixing depths and south-south-westerly flow favored the accumulation of photochemical precursors to the east of the trough (Seaman and Michelson, 2000), further explaining the ozone concentrations exceeding 120 ppb along the northeastern U.S. urban corridor.

The observed data used to verify the model predictions are a subset of the measurements made during the North American Research Strategy for Tropospheric Ozone-Northeast (NARSTO-NE) 1995 intensive field campaign (Mueller, 1998). A total of 327 measurement sites distributed throughout the Northeastern United States were selected to make the model comparison. The modeled and measured ozone concentrations were paired spatially by performing a bi-linear horizontal interpolation of the simulated values to the corresponding monitor location.

Results and Discussion

Modeled and observed maximum 1-h ozone concentrations for the Northeastern U.S. are shown in Figure 11(a) and (b), respectively. In general, good agreement is observed between measured and modeled ozone. The simulation captures the broad

features of the geographical distribution of this episode, but not the detailed spatial variability. In particular, the highest ozone peaks are under-predicted by the model. As given in Table 4, the model shows a raw bias of –9.7 ppb, a normalized bias of –7.3%, a raw gross error of 18.3 ppb, and a normalized gross error of 18.5% for the spatially paired maximum 1-h ozone mixing ratios. Table 4 also shows a complete suite of statistical measures to evaluate the model performance that includes temporally and spatially paired observed and modeled ozone concentrations. These simulation results are within the performance "goals" suggested by Tesche *et al.* (1990) and by Hanna *et al.* (1996).

In order to build further confidence in the ability of the model to predict photochemical species sensitivities to changes in VOC and NO_x, we performed three separate series of runs, each of them with 35% reductions in emission rates for VOC and NO_x. The first simulation (BASECASE) corresponds to the base case scenario with standard emission rates. In the second run (DBLSO2) the SO_2 emissions rates are doubled from those of the base case. In the third scenario (DBLVOC) the anthropogenic VOC emission rates are doubled with respect to the base case. Subsequently, we calculate the values for two indicator ratios, namely O_3/NO_z ($NO_z = NO_y\text{-}NO_x$) and H_2O_2/HNO_3, associated with ozone- NO_x- and VOC-sensitive locations at 16:00 EDT (20:00 UTC). VOC-sensitive locations are defined as those where the O_3 concentration in the simulation with reduced VOC is lower than the levels of O_3 in both the base case scenario and in the simulation with an equivalent reduction in NO_x by at least 5 ppb (Sillman *et al.*, 1997). NO_x-sensitive locations are classified analogously.

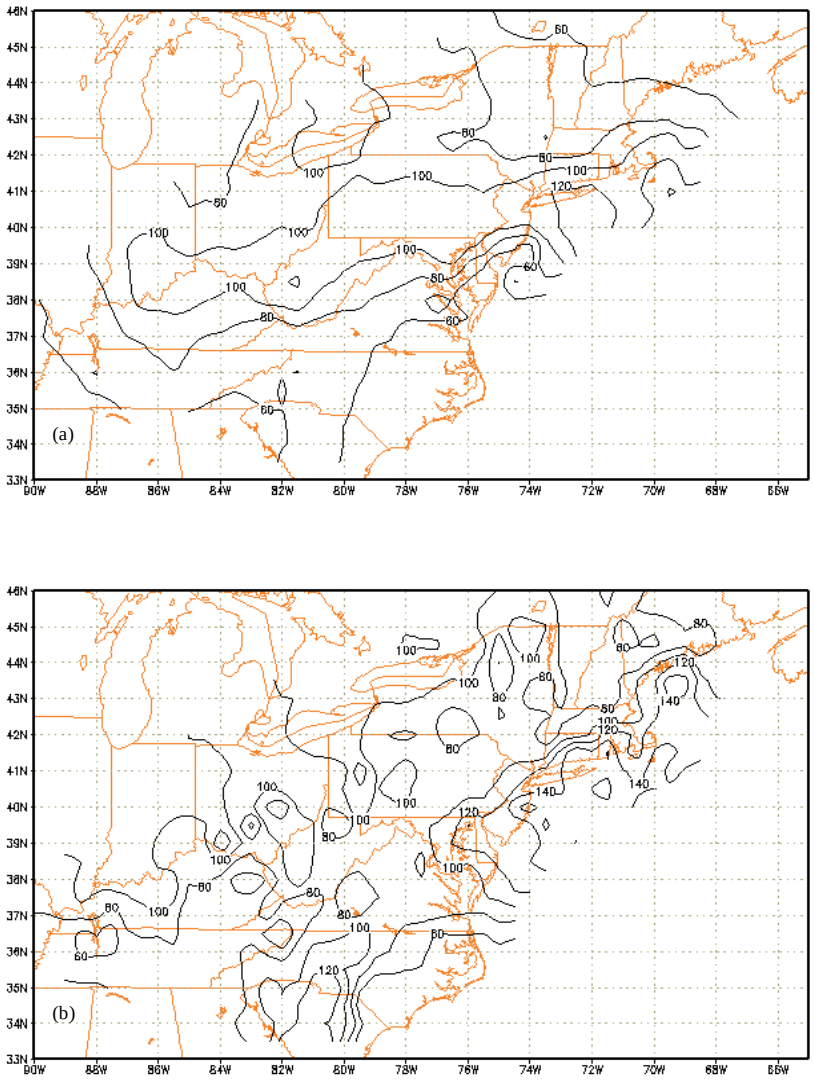

Figure 11: (a) Modeled and (b) observed peak ozone concentrations (ppb) for July 14, 1995.

Table 4: Model performance statistics for O_3.

N		327
1-h Peak	*Raw bias (ppb)*[a]	-9.7
	Norm bias (%)[b]	-7.3
	Raw gross error (ppb)[c]	18.3
	Norm gross error (%)[d]	18.5
Early morning (6-9 AM)	*Raw bias (ppb)*[a]	-1.4
	Raw gross error (ppb)[c]	16.2
Late night (2-5 AM)	*Raw bias (ppb)*[a]	6.4
	Raw gross error (ppb)[c]	18.6
Normalized bias (%)[b]	*O_3>20 ppb*	5.1
	O_3>40 ppb	-6.3
	O_3>60 ppb	-11.8
Raw bias (ppb)[a]	*O_3>20 ppb*	-2.6
	O_3>40 ppb	-7.0
	O_3>60 ppb	-11.3
Normalized gross error (%)[d]	*O_3>20 ppb*	33.4
	O_3>40 ppb	25.7
	O_3>60 ppb	22.5
Raw gross error (ppb)[c]	*O_3>20 ppb*	18.3
	O_3>40 ppb	18.5
	O_3>60 ppb	19.5

[a] Raw bias: $\frac{1}{N}\sum_{i=1}^{N}[C_{p,i}(t) - C_{o,i}(t)]$

[b] Normalized raw bias: $\frac{1}{N}\sum_{i=1}^{N}\frac{[C_{p,i}(t) - C_{o,i}(t)]}{C_{o,i}(t)}$

[c] Raw gross error: $\frac{1}{N}\sum_{i=1}^{N}\left|C_{p,i}(t) - C_{o,i}(t)\right|$

[d] Normalized gross error: $\frac{1}{N}\sum_{i=1}^{N}\frac{\left|C_{p,i}(t) - C_{o,i}(t)\right|}{C_{o,i}(t)}$

where C_p is the modeled concentration and C_o is the measured concentration.

Table 5 shows the median values along with the 5th and 95th percentiles for the indicator ratios corresponding to NO_x-sensitive and VOC-sensitive locations, respectively. As can be inferred from Table 5, the values obtained in these calculations are not substantially different from those calculated by Sillman (1995; 1997). NO_x-sensitive locations are associated with $O_3/NO_z > 12$ and $H_2O_2/HNO_3 > 0.5$, while VOC-sensitive stations are linked to $O_3/NO_z < 9$ and $H_2O_2/HNO_3 < 0.3$.

Following Sillman (1995), we used the $\{[H_2O_2]+[SO_4^{2-}]\}/\{[HNO_3]+[NO_3^-]\}$ ratio as an indicator for the sensitivity of potential sulfate to changes in NO_x and VOC emissions. Figure 12 depicts the potential SO_4^{2-}-VOC-NO_x sensitivity for the BASECASE simulation at 16:00 EDT (20:00 UTC). This figure shows the mixing ratio and percentage normalized reduction in $\{[H_2O_2]+[SO_4^{2-}]\}$ concentration as a consequence of either a NO_x or a VOC emission reduction for each grid within the model domain. The change in potential sulfate is plotted as a function of the concurrent $\{[H_2O_2]+[SO_4^{2-}]\}/\{[HNO_3]+[NO_3^-]\}$ ratio. As can be inferred, there is well-defined contrast between NO_x and VOC sensitive locations. High $\{[H_2O_2]+[SO_4^{2-}]\}/\{[HNO_3]+[NO_3^-]\}$ ratios are associated with reductions in $\{[H_2O_2]+[SO_4^{2-}]\}$ concentrations as NO_x emissions are reduced, while no sensitivity is observed for changes in VOC (NO_x sensitive regime). On the other hand, low indicator ratios are linked to a decrease in "potential" sulfate as the VOC emissions are reduced and an *increase* in the $\{[H_2O_2]+[SO_4^{2-}]\}$ concentrations when the NO_x emissions decrease (VOC sensitive regime).

Table 5: Distribution of ozone sensitivity indicator values.

Indicator / run	VOC sensitive *50th percentile*	*locations* *95th percentile*	*NO_x sensitive* *5th percentile*	*locations* *50th percentile*
H_2O_2/HNO_3				
BASECASE	0.16	0.21	0.49	1.30
DBLSO2	0.17	0.22	0.57	1.83
DBLVOC	0.14	0.30	0.70	2.22
Sillman *et al.*(1997)	(0.13-0.33)	(0.24-0.59)	(0.28-0.68)	(0.73-1.58)
O_3/NO_z				
BASECASE	8.3	9.6	12.3	25.7
DBLSO2	8.4	9.7	12.4	25.7
DBLVOC	6.8	9.6	12.7	25.8
Sillman *et al.*(1997)	(5.8-8.6)	(7.7-10.4)	(7.9-11.9)	(11.8-17.7)

The correspondence between the SO_4^{2-}-VOC-NO_x sensitivity and the indicator ratio was evaluated quantitatively by calculating the 5th, 50th, and 95th percentiles for the $\{[H_2O_2]+[SO_4^{2-}]\}/\{[HNO_3]+[NO_3^-]\}$ ratios associated with VOC- and NO_x-sensitive locations (Table 6). We define NO_x-sensitive locations as those where the normalized $\{[H_2O_2]+[SO_4^{2-}]\}$ calculated in the simulation with a 35% reduction in NO_x is lower than the normalized potential sulfate concentrations modeled with a 35% reduction in VOC by at least 5%. VOC-sensitive stations are defined in an analogous way. Table 6 shows that the median values of the $\{[H_2O_2]+[SO_4^{2-}]\}/\{[HNO_3]+[NO_3^-]\}$ ratios linked to NO_x sensitive stations are at least four times higher than those associated with VOC-sensitive locations. The 95th percentile of the collection of indicator values corresponding to VOC-sensitive stations along with the 5th percentile of indicator values associated with NO_x-sensitive locations identify the threshold $\{[H_2O_2]+[SO_4^{2-}]\}/\{[HNO_3]+[NO_3^-]\}$ ratio for the transition from VOC to NO_x sensitivity. We find similar transition points for the three different model scenarios that range between 1.4 to 2.2. In order to visualize the geographical distribution of the VOC-sensitive locations for July 14 at 20:00 UTC, we have created isopleths for indicator values lower than 1 (Figure 13). In general, these stations are situated downwind of major urbanized areas such as the Northeast corridor, Detroit, Toronto, and Chicago, a fact reflecting the geographical location of strong NO_x sources.

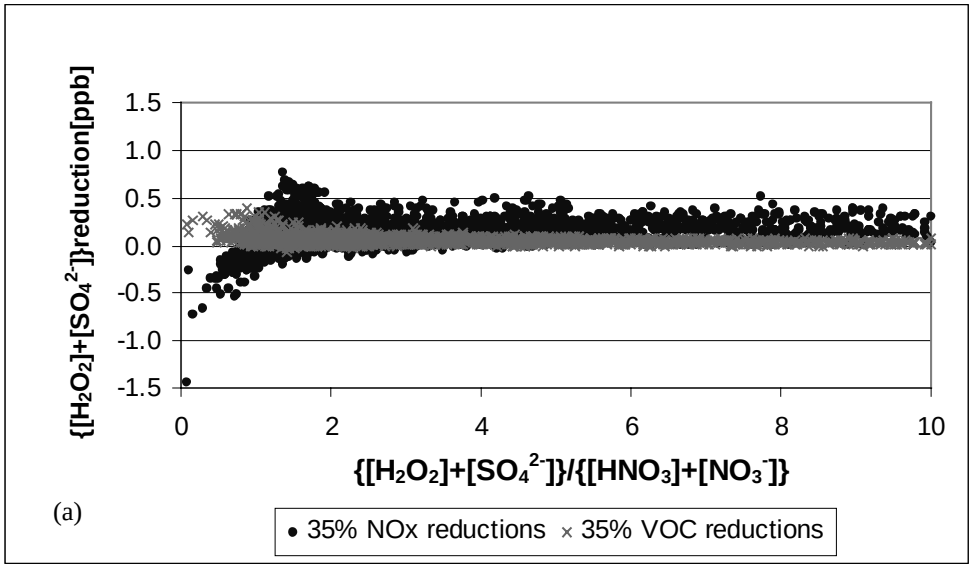

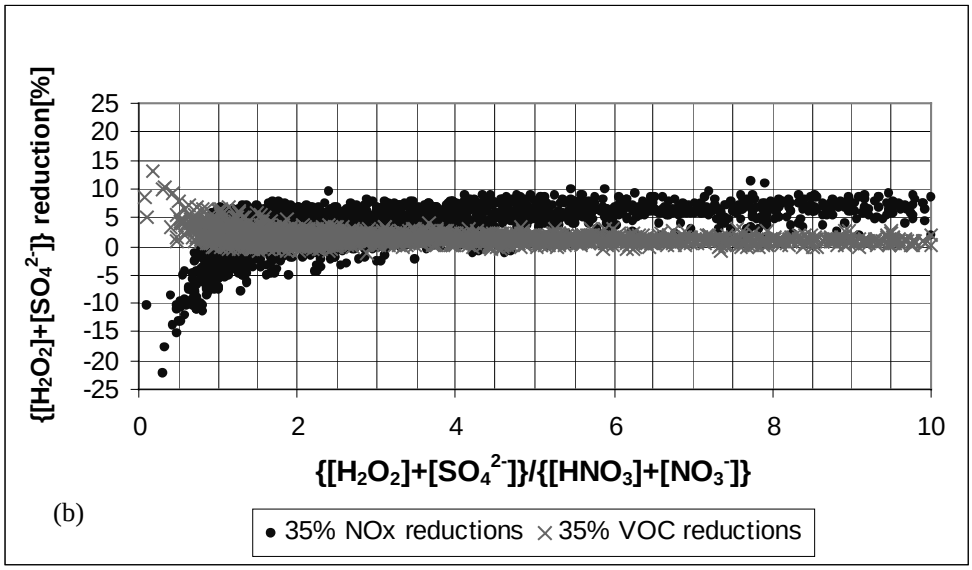

Figure 12: (a) Mixing ratio (ppb) and (b) normalized percentage response of potential sulfate concentrations to changes in NO_x and VOC versus $\{[H_2O_2]+[SO_4^{2-}]\}/\{[HNO_3]+[NO_3^-]\}$ ratios for 20:00 UTC, July 14, 1995.

Table 6: Distribution of $\{[H_2O_2]+[SO_4^{2-}]\}/\{[HNO_3]+[NO_3^-]\}$ ratios for NO_x- and VOC-sensitive regimes.

Run	VOC sensitive 5^{th} percentile	VOC sensitive 50^{th} percentile	*locations* 95^{th} *percentile*	*NO_x sensitive locations* 5^{th} *percentile*	50^{th} *percentile*	95^{th} *percentile*
BASECASE	0.47	0.96	1.82	1.54	7.30	18.66
DBLSO2	0.30	0.89	1.37	1.73	4.76	16.86
DBLVOC	0.65	1.23	2.25	1.60	7.46	20.16

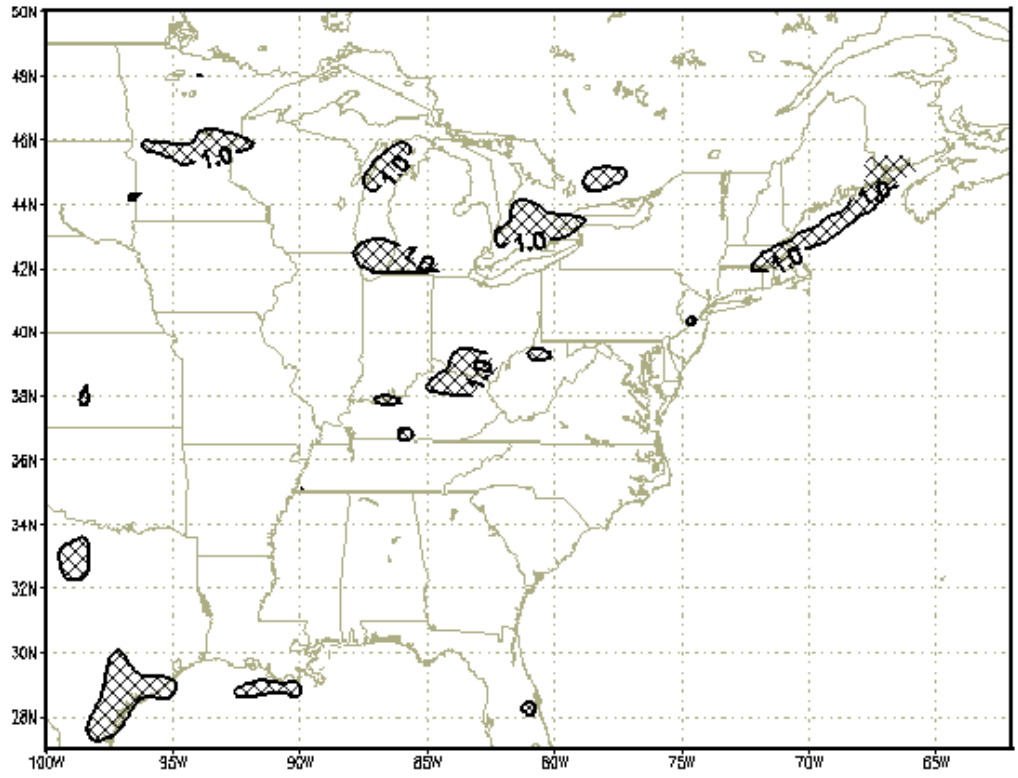

Figure 13: Geographical distribution of the VOC-sensitive locations for July 14, 1995 at 20:00 UTC. Shaded regions correspond to indicator values lower than 1.

Chapter 6

SUMMARY AND CONCLUSIONS

Throughout this dissertation different aspects of the relationship between ambient measurements, laboratory experiments and atmospheric modeling has been explored with increasing levels of complexity. The main emphasis of this relationship has been focused on the simulation aspects of a variety of pollution phenomena such as the dispersion of non-reacting pollutants emitted from a smokestack, the forecast of tropospheric ozone formation over a regional scale, and the sensitivity of sulfate aerosol to changes on NO_x and hydrocarbon source strength.

The relationship (Equation 2-12) derived in Chapter 2 provides a link between the inherent uncertainty in pollutant dispersion in laboratory and ABL flows. This method can be used to estimate the expected deviation of observed concentrations of pollutants from predicted ensemble means in the ABL based on laboratory-derived inherent uncertainties. The large time and length scales of turbulence in the ABL cause large inherent uncertainty in time-averaged concentration measurements in pollutant-dispersion problems. We showed that for the same averaging time the inherent uncertainty in laboratory models of atmospheric flow is apt to be much less. This is consistent with the experience that laboratory studies can give insights into the behavior of pollutant

dispersion that are difficult to obtain directly from the atmosphere (Lamb, 1982; Thompson *et al.*, 2000). For instance, the now generally accepted non-Gaussian mean concentration profiles in the vertical downwind of sources in the convective ABL were first observed in tank experiments (Willis and Deardorff, 1978). Those experiments guided the design of field campaigns such as the Convective Diffusion Observed by Remote Sensors (CONDORS) experiment (Briggs, 1993).

Fluid modeling has been underutilized in assessing inherent uncertainty in dispersion, and within its limitations (e.g., Reynolds number similarity) it provides a unique practical way to estimate it in some problems. Further measurements in the ABL are needed in order to provide empirical proof of the findings presented in this work.

On the other hand, in Chapter 3 a three-dimensional hybrid model has been implemented to forecast summertime ozone concentrations over the northeastern United States. The calculated ozone concentrations have been compared against observational data at a number of monitoring stations. Generally, a fair agreement is observed at most stations, especially taking into account the large number of assumptions used to construct the model. HY-SPLIT CheM is the first operational implementation of the particle-in-grid approach applied to air quality modeling (Stohl, 1998). This model constitutes a feasible tool due to its simplicity and low cost of implementation. Nevertheless, despite the encouraging results obtained here, further investigation is necessary to establish the range of applicability and the limitations of the model.

In Chapter 4 we investigated a case study in which a large abundance of ambient SO_4^{2-} was measured in the air prior to a heavy rain event loaded with high concentrations

of H_3O^+ and SO_4^{2-} in Central Pennsylvania (Stein and Lamb, 2000). This study has revealed that huge acid deposition events are possible even after the major reductions in SO_2 emissions that have occurred as a consequence of the Clean Air Act Amendments of 1990 (Lynch *et al.*, 2000). The present work has been introduced in order to gain insight into the chemical and physical processes that lead to the formation of SO_4^{2-} in the ambient aerosol and in rain. For the most part, the large concentrations of sulfate found in the precipitation of high-deposition events, as in the case studied in Chapter 4, are derived from ambient sulfate formed prior to a convective rain event. This preformed SO_4^{2-} most likely formed in upwind, non-precipitation clouds via the aqueous-phase oxidation of SO_2 by H_2O_2 in limited supply.

Furthermore, a theoretical analysis of the sulfate-formation pathways to investigate the relationship between the SO_2 oxidants concentrations and their precursors, NO_x and VOC, was introduced in Chapter 5. This analysis provided the theoretical rationale for using the ratio of $\{[H_2O_2]+[SO_4^{2-}]\}/\{[HNO_3]+[NO_3^-]\}$ as the indicator for "potential" SO_4^{2-}-VOC-NO_x sensitivity. The concentrations of these indicator species were calculated from a series of photochemical model simulations with varying rates of NO_x and VOC emissions using a three-dimensional Eulerian model (MODELS-3) that covers the northeastern United States. It was shown that a correlation indeed exists between potential sulfate NO_x-VOC-sensitivity and simulated afternoon values of the $\{[H_2O_2]+[SO_4^{2-}]\}/\{[HNO_3]+[NO_3^-]\}$ ratio. The threshold value for the transition between NO_x and VOC sensitive regimes seems to be robust despite the different emission conditions used to simulate the episode introduced in Chapter 5. Potential ambient sulfate

is likely to decrease as NO_x emissions are reduced when the indicator species ratio is higher than approximately 2. Values lower than 1.5 for this non-dimensional indicator identify stations associated with a VOC-sensitive regime. Under this regime, a decrease in NO_x emissions would lead to an *increase* in sulfate formation. This counter-intuitive result arises as consequence of a highly nonlinear and coupled behavior of the atmospheric chemical processes involved in the sulfate formation.

The use of photochemical indicators to identify NO_x- or VOC- sensitive locations provides valuable information for the decision-making and model-validation processes. This technique could also help with assessments of the impact of reducing other primary pollutant sources on ambient aerosol sulfate. Although the magnitude of the response of potential sulfate to changes in VOC and NO_x sources strength is not overwhelming (±10% for most stations for a 35% reduction in emissions), it is important to be aware of the sensitivity of the chemical system in order to avoid unexpected increases in sulfate concentrations. Some caveats should also be mentioned about the limitations to the applicability of the sulfate sensitivity indicator. Dry deposition, for instance, influences the concentrations of the indicator species in non chemical ways. Consequently, afternoon indicator values should be used to minimize such effects. Also, no attempt has been made here to evaluate the influence of variations in actinic flux (e.g., due to the presence of clouds) on the indicator values. Future studies should include measurements of hydrogen peroxide, sulfate, nitric acid, and particulate nitrate to confirm the effect of NO_x or VOC emissions reduction on the formation of sulfate.

REFERENCES

AIRSweb, 1998. Aerometric Information Retrieval System (AIRS) administered by the U.S.E.P.A., Office of Air Quality Planning and Standards, Information Transfer and Program Integration Division, located in Research Triangle Park, North Carolina. http://www.epa.gov/aqspubl1/annual_summary.html

Binkowski F.S. and Shankar U., 1995. The regional particulate model 1. Model decription and preliminary results. *Journal of Geophysical Research*, **100** (D12), 26191-26209.

Briggs, G.A., 1993: Final results of the CONDORS convective diffusion experiment. *Boundary-Layer Meteorology* **62**, 315-328.

Brunekreef B., Dockery D.W., and Krzyzanowski M., 1995. Epidemiologic studies on short-term effects of low levels of major ambient air pollution components, *Environmental Health Perspectives*, **103** (Suppl. 2), S3-S13.

Byun D.W. and Dennis R., 1995. Design artifacts in Eulerian air quality models: evaluation of the effects of layer thickness and vertical profile correction on surface ozone concentrations. *Atmospheric Environment* **29** (1), 105-126.

Calvert J.G., Su F., Bottenheim J.W., and Strausz O.P., 1978. Mechanism of the homogeneous oxidation of sulfur dioxide in the troposphere. *Atmospheric Environment* **12**, 197-226.

Cardelino C.A., and Chameides , 1990. Natural hydrocarbons, urbanization, and urban ozone. *Journal of Geophysical Research* **95**, 13971-13979.

Chang J. S., F. S. Binkowski, N. L. Seaman, D. R. Stauffer, W. R. Stockwell, C. J. Walcek, S. Madronich, P. Middleton, J. E. Pleim, H. H. Landsford, 1990. The regional acid deposition model and engineering model. State of Science/TechnologyReport 4, National Acid Precipitation Assessment Program, 722 Jackson Place, NW Washington D. C. 20503.

Charlson R.J., Langner J., Andreae M.O., and Warren S.G., 1991. Perturbation of the northern hemisphere radiative balance by backscattering from antropogenic sulfate aerosols. *Tellus* **43** (Ser. A-B), 152-163.

Chock D.P., and Winkler S.L., 1994. A particle grid air quality modeling approach, 2. Coupling with chemistry. *Journal of Geophysical Research* **99** (D1), 1033-1041.

Dab W., Segala C., Dor F., Festy B., Lameloise P., Le Moullec Y., Le Tertre A., Medina S., Quenel P., Wallaert B., and Zmirou D., 2001. Air pollution and health: Correlation or causality? The case of the relationship between exposure to particles and cardiopulmonary mortality. *Journal of the Air & Waste Management Association* **51**, 220-235.

Daum P.H., Kelly T.J., and Schwartz S.E., 1984. Measurements of the chemical composition of stratiform clouds. *Atmospheric Environment* **18**, 2671-2684.

Dennis R.L., Byun D.W., Novac J.H., Galluppi K.J., Coats C.J., and Vouk M.A., 1996. The next generation of integrated air quality modeling: EPA's MODELS-3. *Atmospheric Environment* **30** (12), 1925-1938.

Dennis R.L., McHenry J.N., Barchet W.R., Binkowski F.S., and Byun D.W., 1993. Correcting RADM's sulfate underprediction: discovery and correction of model errors and testing the corrections through comparisons against field data. *Atmospheric Environment* **27A** (6), 975-997.

Dickerson R.R., Kondragunta S., Stenchikov G., Civerolo K.L., Doddridge B.G., and Holben B.N., 1997. The impact of aerosols on solar ultraviolet radiation and photochemical smog. *Science* **278**, 827-830.

Draxler, R.R. and Hess G.D., 1997. Description of the HYSPLIT_4 modeling system, NOAA Technical Memorandum ERL ARL-224, December, 24 pp. [Available from National Technical Information Service, 5285 Port Royal Road, Springfield, VA 22161.]

Draxler, R.R, and Hess G.D., 1998. An overview of the HY-SPLIT_4 modelling system for trajectories, dispersion, and deposition. *Australian Meteorological Magazine* **47**, 295-308.

Dutkiewicz V.A., Burkhard E.G., and Husain L., 1995. Availability of H_2O_2 for oxidation of SO_2 in clouds in the northeastern United States. *Atmospheric Environment* **29** (22), 3281-3292.

Dutkiewicz V. A. and Husain L., 1998. Inefficient scavenging of aerosol sulfate by non-precipitating clouds in polluted air. *Atmospheric Environment* **32** (16), 2793-2801.

Eggleton A.E.J. and Cox R.A., 1978. Homogeneous oxidation of sulphur compounds in the atmosphere. *Atmospheric Environment* **12**, 227-230.

EPA, 1996a. Environmental Protection Agency, Air quality criteria for particulate matter, Vol. 1; EPA/600/P-95/001aF; Office of research and development: Washington, DC.

EPA, 1996b. Environmental Protection Agency, Office of Mobile Sources: User's Guide for MOBILE 5a (Mobile Source Emission Factor Model), EPA-AA-TEB-92-01, 176 pp.

EPA, 1999a Environmental Protection Agency. ftp:/www.epa.gov/pub/scram001/modelingcenter/NOxSIPcall/emissions

EPA, 1999b. Environmental Protection Agency, Science Algorithms of the EPA MODELS-3 community Multiscale Air Quality (CMAQ) Modeling System, EPA/600/R-99/030. Office of Research and Development: Washington, DC 20460.

Finlayson-Pitts B.J. and Pitts J.N. Jr., 1986. Atmospheric chemistry: fundamentals and experimental techniques. John Wiley and Sons, Inc, 1098 pp.

Fox, D., 1984: Uncertainty in air quality modeling. *Bulletin of the American Meteorological Society* **65**, 27-36.

Gery M.W., Whitten G.Z., Killus J.P., and Dodge M.C., 1989. A photochemical kinetics mechanism for urban and regional scale computer modeling. *Journal of Geophysical Research* **94** (D10), 12925-12956.

Gery M.W. and Crouse R.R., 1991. User's guide for executing OZIPR, project summary. Research Triangle Park, NC, U.S. Environmental Protection Agency, Atmospheric Sciences Research Laboratory, 166 pp.

Gear C.W., 1971. Numerical initial value problems in ordinary differential equations, Prentice-Hall, New Jersey, 253 pp.

Grell G.A., Dudhia J., and Stauffer D.R., 1994. A description of the Fifth-Generation Penn State/NCAR Mesoscale Model (MM5). NCAR Tech. Note, NCAR/TN-398+STR, 122 pp.

Hanna S.R., Moore G.E., and Fernau M.E., 1996. Evaluation of photochemical grid models (UAM-IV, UAM-V, and the ROM/UAM-IV Couple) using data form the Lake Michigan Ozone Study (LMOS). *Atmospheric Environment* **30** (19), 3265-3279.

Hegg D.A. and Hobbs P.V., 1986. Sulfate and nitrate chemistry in cumuliform clouds. *Atmospheric Environment* **20** (5), 901-909.

Hegg D.A. and Hobbs P.V., 1988. Comparisons of sulfate and nitrate production in clouds on the Mid-Atlantic and Pacific northwest coasts of the United States. *Journal of Atmospheric Chemistry* **7**, 325-333.

Hegg D.A., Hobbs P.V., and Radke L., 1984. Measurements of the scavenging of sulfate and nitrate in clouds. *Atmospheric Environment* **18** (9), 1939-1946.

Hertel O., Christensen J., Runge E.H., Asman W.A.H., Berkowicz R., and Hovmand M.F., 1995. Development and testing of a new variable scale air pollution model – ACDEP. *Atmospheric Environment* **29** (11), 1267-1290.

Hidy G.M., Hales J.M., Roth P.M., and Scheffe R., 2000. Fine particles and oxidant pollution: Developing an agenda for cooperative research. *Journal of the Air & Waste Management Association*, **50**, 613-632.

Hoke J.E., Phillips N.A., DiMego G.J., Tuccillo J.J, and Sela J.G., 1989. The regional analysis and forecast system of the National Meteorological Center. *Weather Forecast* **4**, 323-334.

Jacob D.J, 1986. Chemistry of OH in remote clouds and its role in the production of formic acid and peroxymonosulfate. *Journal. of Geophysical Research* **91** (D9), 9807-9826.

Jacob D.J., Logan J.A., Yevich R.M, Gardner G.M., Spivakovsky C.M., Wofsy S.C., Munger J.W., Sillman S., Prather M.J., Rodgers M.O., Westberg H., and Zimmerman P.R., 1993. Simulation of summertime ozone over North America. *Journal of Geophysical Research* **98** (D8), 14797-14816.

Karamchandani P. and Venkatram A., 1992. The role of non-precipitating clouds in producing ambient sulfate during summer: results from simulations with the acid deposition and oxidation model (ADOM). *Atmospheric Environment* **26A** (6), 1041-1052.

Kleinman L.I. and Daum P.H., 1991. Oxidant limitation to the formation of H_2SO_4 near a SO_2 source region. *Atmospheric Environment* **25A**, 2023-2028.

Kleinman L.I., 1991. Seasonal dependence of boundary layer peroxide concentration: the low and high NO_x regimes. *Journal of Geophysical Research* **96** (D11), 20721-20733.

Kreyszig E., 1967. Advanced Engineering Mathematics, 2nd ed., Wiley, New York, 898 pp.

Lamb, R.G., 1982. Diffusion in the convective boundary layer, in F.T.M Nieuwstadt and H. van Dop (eds.), Atmospheric Turbulence and Air Pollution Modelling. D. Reidel Publishing Company, 358 pp.

Lamb D. and Comrie L., 1993. Comparability and precision of MAP3S and NADP/NTN precipitation chemistry data at an acidic site in eastern North America. *Atmospheric Environment* **27A**, 1993-2008.

Lynch J.A., Bowersox V.C., and Grimm J.W., 2000. Changes in atmospheric deposition in eastern USA following enactment of Title IV of the Clean Air Act Amendments of 1990, *Atmospheric Environment* **34**,1665-1680.

MacCracken M.C, 1978. MAP3S: An investigation of atmospheric, energy related pollutants in the northeastern United States. *Atmospheric Environment* **12**, 649-659.

Malm W.C., Trijonis J., Sisler J., Pitchford M., and Dennis R.L., 1994. Assessing the effect of SO_2 emission changes on visibility. *Atmospheric Environment* **28A**, 1023-1034.

Mathur R., Saylor R.D., and Peters L.K., 1992. The STEM-II regional scale acid deposition and photochemical oxidant model- IV. The impact of emission reductions on mesoscale acid deposition in the lower Ohio River valley. *Atmospheric Environment* **26A** (5), 841-861.

McHenry J.N. and Dennis R.L, 1994. The relative importance of oxidation pathways and clouds to atmospheric ambient sulfated production as predicted by the regional acid deposition model. *Journal of Applied Meteorology* **33**, 890-905.

McHenry J.N., Seaman N., Coats C., Stauffer D., Lario-Gibbs A., Vukovich J., Hayes E., and Wheeler N.. The NCSC-PSU numerical air quality prediction project: Initial evaluation, status, and prospects. Symposium on Interdisciplinary Issues and Atmospheric Chemistry Issues, January 2000.

Milford J.B., Gao D., Sillman S., Blossey P., and Russell A.G., 1994. Total reactive nitrogen (NOy) as an indicator of the sensitivity of ozone to reductions in hydrocarbon and NO_x emissions. *Journal of Geophysical Research* **99** (D2), 3533-3542.

Misra P.K., Bloxam R., Fung C, and Wong S., 1989. Non-linear response of wet deposition to emission reduction: a model study. *Atmospheric Environment* **23** (3), 671-687.

Mueller P.K., 1998. NARSTO 1998 Model-Intercomparison study verification data: NARSTO-Northeast 1995 surface ozone, NO, and NO_x. Available online from the Langley Atmospheric Sciences Data Center, NASA Langley Research Center, Hampton, Virginia, U.S.A.

NAPAP, 1993. National Acid Precipitation Assessment Program, 1992 Report to Congress. 130 pp.

National Emission Trends Viewer Version 2.0 CD, 1998, EPA/454/C-98-003.

Pandis S.N. and Seinfeld J.H., 1989. Mathematical modeling of acid deposition due to radiating fog. *Journal of Geophysical Research* **94**, 12911-12923.

Penkett S.A., Jones B.M.R., Brice K.A., and Eggleton, 1979. The importance of atmospheric ozone and hydrogen peroxide in oxidizing sulfur dioxide in cloud and rainwater. *Atmospheric Environment* **13**, 123-137.

Philips N.A., 1975. The Nested Grid Model, NOAA Tech. Rep. NWS-22, National Weather Service, Silver Spring, MD.

Pierce T., Geron Ch., Bender L., Dennis R., Tonnesen G., Guenther A., 1998. Influence of increased isoprene emissions on regional ozone modeling. *Journal of Geophysical Research* **103** (D19): 25611-25629.

Press W.H., Teukolsky S.A., Vetterling W.T., and Flannery B.P., 1992. Numerical Recipies: the art of scientific computing, Cambridge University Press, N.Y.

Pruppacher H.R. and Klett J.D., 1997. Microphysics of Clouds and Precipitation. Kluwer Academic Publishers, Dordrecht/Boston/London, 954 pp.

Rolph G.D., Draxler R.R., and de Pena R.G., 1992. Modeling sulfur concentrations and depositions in the United States during ANATEX. *Atmospheric Environment* **26A** (1), 73-93.

Rolph G.D., Draxler R.R., and de Pena R.G., 1993. The use of model-derived and observed precipitation in long-term sulfur concentration and deposition modeling. *Atmospheric Environment* **27A** (13), 2017-2037.

Rothert J., Bowersox V., and Artz R., 1997. The NADP Atmospheric Integrated Research Monitoring Network-wet (NADP/AIRMoN-wet): Site Operator's Manual. NOAA Technical Memorandum ERL ARL-222, Air Resources Laboratory, Silver Spring, MD, April 1997, 38 pp.

Sakugawa H., Kaplan I.R., Tsai W., and Cohen Y., 1990. Atmospheric hydrogen peroxide. Does it share a role with ozone in degrading air quality? *Environmental Science & Technology* **24** (10), 1452-1462.

Seaman N.L. and Michelson S.A, 2000. Mesoscale meteorological structure of a High-ozone episode during the 1995 NARSTO-Northeast study. *Journal of Applied Meteorology*, **39**, 384-398.

Seinfeld J.H. and Pandis S.N., 1998. Atmospheric chemistry and physics. From air pollution to climate change. John Wiley & sons, Inc., New York, 1326 pp.

Shin W-Ch., and Carmichael G.R., 1992. Sensitivity of acid production/deposition to emission reductions. *Environmental Science and Technology* **26** (4), 715-725.

Shin W.C. and Carmichael G.R., 1992. Analysis of wet deposition in the eastern United States. *Atmospheric Environment* **26A** (3), 465-484.

Shreffler J.H. and Barnes H.M., 1996. Estimation of trends in atmospheric concentrations of sulfate in the northeastern United States. *Journal Air & Waste Management Association* **46**, 621-630.

Sillman S., 1995. The use of NO_y, H_2O_2, and HNO_3 as indicators for ozone-NO_x-hydrocarbon sensitivity in urban locations. *Journal of Geophysical Research* **100** (D7), 14175-14188.

Sillman S., Logan J.A., and Wofsy S.C., 1990. The sensitivity of ozone to nitrogen oxides and hydrocarbons in regional ozone episodes. *Journal of Geophysical Research* **95** (D2), 1837-1851.

Sillman S., He D., Cardelino C., and Imhoff R.E., 1997. The use of photochemical indicators to evaluate ozone-NO_x-Hydrocarbon sensitivity: Case studies from Atlanta, New York, and Los Angeles. *Journal of the Air & Waste Management Association* **47**, 1030-1040.

Sistla G., Hao W., Ku J-Y., Kallos G., Zhang K., Mao H., and Rao S.T., 2001. An operational evaluation of two regional-scale ozone air quality modeling systems over the eastern United States. *Bulletin of the American Meteorological Society* **82**, 945-964.

Snyder, W.H., 1981: Guideline for fluid modeling of atmospheric diffusion. Environmental Sciences Research Laboratory, U.S. Environmental Protection Agency, Research Triangle Park, NC, Report EPA-600/8-81-009, 185 pp.

Spellmann J.W. and Hindmarsh A.C., 1975. GEARS: Solution of Ordinary Differential Equations Having a Sparse Jacobian Matrix, California Univ., Livermore Lawrence Livermore Lab., pp. 41.

Stein A.F. and Lamb D., 2000. The Sensitivity of Sulfur Wet Deposition to Atmospheric Oxidants. *Atmospheric Environment* **34**, 1681-1690.

Stein A.F., Lamb D., and Draxler R.R., 2000. Incorporation of detailed chemistry into a three-dimensional lagrangian-eulerian hybrid model: application to regional tropospheric ozone. *Atmospheric Environment* **34** (25) 4361-4372.

Stein A.F. and Wyngaard J.C., 2001. Fluid Modeling and Evaluation of Inherent Uncertainty. *Journal of Applied Meteorology* **40** (10), 1769-1774.

Stein A.F. and Lamb D., 2001. Chemical Indicators of Sulfate Sensitivity to Nitrogen Oxides and Volatile Organic Compounds. *Journal of Geophysical Research* (submitted).

Stockwell W.R., 1994a. The effect of gas-phase chemistry on aqueous-phase sulfur dioxide oxidation rates. *Journal of Atmospheric Chemistry* **19**, 317-329.

Stockwell W.R., 1994b. Communication concerning 'The role of clouds in tropospheric photochemistry' by Lelieveld and Crutzen. *Journal of Atmospheric Chemistry* **18**, 397-399.

Stockwell W.R. and Calvert J.G., 1983. The mechanism of the HO-SO_2 reaction. *Atmospheric Environment* **17**, 2231-2235.

Stockwell W.R., Middleton P., and Chang J.S., 1990. The second generation regional acid deposition model chemical mechanism for regional air quality modeling. *Journal of Geophysical Research* **95** (D10), 16343-16367.

Stohl A., 1998. Computation, accuracy and applications of trajectories – A review and bibliography. *Atmospheric Environment* **6**, 947-966.

Tanner R.L., D'Ottavio T., Garber R.W., and Newman L., 1980. Determination of ambient aerosol sulfur using a continuous flame photometric detection system. I. Sampling system for aerosol sulfate and sulfuric acid. *Atmospheric Environment* **13**, 121-127.

Tennekes, H. and J.L. Lumley, 1972. A first course in turbulence. The MIT Press. Cambridge, MA, 300 pp.

Tesche T.W., Georgopoulos P., Seinfeld J.H., Lurmann F., and Roth P.M., 1990. Improvement in procedures for evaluating photochemical models. Report A832-103, California Air Resources Board, Sacramento, California.

Thompson, R.S., W.H. Snyder, and J.C. Weil, 2000: Laboratory simulation of the rise of buoyant thermals created by open detonation. *Journal of Fluid Mechanics* **417**, 127-156.

Townsend, A.A., 1956. The structure of turbulent shear flow. Cambridge University Press, 315 pp.

Trainer M., Buhr M.P., Curran C.M., Fehesenfeld F.C., Hsie E.Y., Liu S.C., Norton R.B., Parrish D.D., Williams E.J., Gandrud B.W., Ridley B.A. Shetter J.D., Allwine E.J., and Westberg H.H., 1991. Observations and modeling of the reactive nitrogen photochemistry at a rural site. *Journal of Geophysical Research* **96** (D2), 3045-3063.

Tremmel H.G., Junkermann W., Slemr F., and Platt U., 1993. On the distribution of hydrogen peroxide in the lower troposphere over the Northeastern United States during late Summer 1988. *Journal of Geophysical Research* **98** (D1), 1083-1099.

Twomey D.J., Piepgrass M., and Wolfe T.L., 1984. An assessment of the impact of pollution on global cloud albedo. *Tellus* **36** (Ser. B), 356-366.

Van Valin C.C., Luria M., Ray J.D., and Boatman J.F., 1991. A comparison of surface and airborne trace gas measurements at a rural Pennsylvania site. *Journal of Geophysical Research* **96** (D11), 20745-20754.

Venkatram, A., 1979. The expected deviation of observed concentrations from a predicted ensemble means. *Atmospheric Environment* **13**, 1547-1549.

Venkatram, A., 1984. The uncertainty in estimating dispersion in the convective boundary layer. *Atmospheric Environment* **18**, 307-310.

Venkatram, A., 1988. Inherent uncertainty in air quality modeling. *Atmospheric Environment* **22**, 1221-1227.

Venkatram, A. and J.C. Wyngaard, 1988. Lectures on air pollution modeling. American Meteorological Society, Boston, MA, 390 pp.

Waggoner A.P., Weiss R.E., Ahlquist, N.C., Covert, D.S., Will S., and Charlson, R.J., 1981. Optical characteristics of atmospheric aerosols. *Atmospheric Environment* **15**, 1891-1909.

Wang Ch. and Crutzen P.J., 1995. Impact of a simulated severe local storm on the redistribution of sulfur dioxide. *Journal of Geophysical Research* **100** (D6), 11357-11367.

Wangteng T., Cohen Y., Sakugawa H., and Kaplan I.R., 1991. Hydrogen peroxide levels in Los Angeles: a screening-level evaluation. *Atmospheric Environment* **25B**, 67-78.

Weil, J.C., R.I. Sykes, and A. Venkatram, 1992. Evaluating air-quality models: Review and outlook. *Journal of Applied Meteorology* **31**, 1121-1145.

Weinstein-Lloyd J.B., Lee J.H., Daum P.H., Kleinman L.I., Nunnermacker L.J., Springston S.R., and Newman L., 1998. Measurements of peroxides and related

species during the 1995 summer intensive of the Southern Oxidants Study in Nashville, Tennessee. *Journal of Geophysical Research* **103** (D17), 22361-22373.

Wesely M.L. and Hicks B.B., 1977. Some factors that affect the deposition rates of sufur dioxide and similar gases on vegetation. *Journal of Air Pollution Control Association* **27**, 1110-1116.

Whitby K.T., 1978. The physical characterization of sulfur aerosols. *Atmospheric Environment* **12**, 135-159.

Willis, G.E., and J.W. Deardorff, 1976. A laboratory model of diffusion into the convective planetary boundary layer. *Quarterly journal of the Royal Meteorological Society* **102**, 427-445.

Willis, G.E. and J.W. Deardorff, 1978. A laboratory study of dispersion from an elevated source within a modeled convective planetary boundary layer. *Atmospheric Environment* **12**, 1305-1311.

VITA

Ariel F. Stein

Education:

- Cordoba, Argentina, June, 1994. Undergraduate Studies: Licenciate in Chemistry (specialization in Physical Chemistry) 5 years degree, College of Chemistry, National University of Cordoba.
- State College, USA, August, 1998. Master in Science, Environmental Pollution Control. Department of Meteorology, The Pennsylvania State University.
- State College, USA. Ph.D in Meteorology. Department of Meteorology, The Pennsylvania State University.

Awards and Honors:

- Second outstanding student. College of Chemistry, National University of Cordoba, Argentina, 1993/94.
- 'Asociación Química Argentina' (Argentine Chemistry Society) Award, Buenos Aires, Argentina, 1994.
- 'Premio Universidad' National University of Cordoba Award, Cordoba, Argentina, 1994.
- Second place Award. Student Poster Session at the 43rd Anniversary Mid Atlantic States Section Air and Waste Management Association, Philadelphia, USA, 1997.
- Second place Award at the Fourteenth Annual Graduate Exhibition. The Pennsylvania State University, 1999.
- Outstanding Student Paper Award, Atmospheric Sciences Section of the American Geophysical Union, Boston, MA, USA, 2001.

Recent Scientific Publications:

- "The Sensitivity of Sulfur Wet Deposition to Atmospheric Oxidants".

Ariel F. Stein and Dennis Lamb. *Atmos. Environ.*, **34**, 1681-1690, 2000.

- "Incorporation of detailed chemistry into a three-dimensional lagrangian-eulerian hybrid model: application to regional tropospheric ozone".

Ariel F. Stein, Dennis Lamb, and Roland R. Draxler. *Atmos. Environ.*, **34**, 4361-4372, 2000.

- " Fluid Modeling and Evaluation of Inherent Uncertainty".

Ariel F. Stein and John C. Wyngaard. *J. Appl. Meteorol.*, **40**, 1769-1774, 2001.

- "Chemical Indicators of Sulfate Sensitivity to Nitrogen Oxides and Volatile Organic Compounds".

Ariel F. Stein and Dennis Lamb. *J. Geophys. Res.* (submitted).